

COCURRENT EXTRACTION IN A RECIPROCATING PLATE COLUMN

By



SOO HONG NOH, B.Eng.

A Thesis

Submitted to the School of Graduate Studies
in Partial Fulfilment of the Requirements
for the Degree
Master of Engineering

McMaster University

July, 1981

COCURRENT EXTRACTION IN A RECIPROCATING PLATE COLUMN



MASTER OF ENGINEERING (1981)
(Chemical Engineering)

McMASTER UNIVERSITY
Hamilton, Ontario

TITLE: Cocurrent Extraction in a Reciprocating
Plate Column

AUTHOR: Soo Hong Noh, B.Eng. (Yon Sei University,
Korea)

SUPERVISOR: Dr. M.H.I. Baird

NUMBER OF PAGES: (xii), 114

ABSTRACT

Mass transfer performance in cocurrent extraction has been studied in a 5.08 cm I.D. Karr reciprocating plate column.

A model for cocurrent mass transfer in a reciprocating plate column, which uses some of the same concepts that have proven useful in the development of a countercurrent mass transfer model, was experimentally confirmed. The indicator colour change method, which employs an instantaneous chemical reaction in the presence of an indicator, was developed to determine the mass transfer rate in cocurrent extraction and has proven very useful in avoiding the additional mass transfer which is always encountered in the sampling and analysis of exit streams. The local mass transfer rate in the column was also investigated by this method.

The time-averaged pressure drop for single phase (water) flow was measured in the column and has been compared with a quasi-steady model.

ACKNOWLEDGEMENTS

I would like to extend my deep appreciation to Dr. M.H.I. Baird for his continued guidance and suggestions during the course of the experiments and the preparation of the thesis. Discussions and communications between Dr. Baird and Dr. Karr for this work are also appreciated.

I am also grateful to Anil Rohatgi and technicians for their assistance in building the column and the Department of Chemical Engineering for its financial support.

My final acknowledgement is due to my wife and family for their everlasting letters and encouragement in various ways.

TABLE OF CONTENTS

	Page
Abstract	iii
Acknowledgements	iv
List of Figures	vii
List of Tables	ix
Nomenclature and Symbols	xi
CHAPTER 1 INTRODUCTION	1
1.1 Liquid-Liquid Extraction	1
1.2 Characteristics of the Karr Reciprocating Plate Column	3
1.3 Mass Transfer with Instantaneous Chemical Reaction	4
1.4 Karr Reciprocating Plate Extraction Column as a Cocurrent Contactor	6
CHAPTER 2 APPARATUS DESIGN AND EXPERIMENTS	9
2.1 Equipment and Calibration	9
2.2 Preparation and Analysis of Materials	16
2.3 Operating Procedures	23
CHAPTER 3 PRESSURE DROP IN THE KARR COLUMN	26
CHAPTER 4 MASS TRANSFER MEASUREMENT	35
4.1 Operating and Equilibrium Lines	35
4.2 Sampling and Analysis of Exit Streams	38
4.3 Indicator Colour Change Method	41

CHAPTER 5	MASS TRANSFER MODELS	46
5.1	N.T.U. and H.T.U. in Cocurrent Plug Flow	46
5.2	Holdup	48
5.3	Specific Interfacial Area and Drop Size	49
5.4	Mass Transfer Coefficients	53
5.5	Prediction of $\overline{K_o a}$ and Column Height	56
CHAPTER 6	MASS TRANSFER RESULTS AND DISCUSSIONS	58
6.1	Effect of ϕ on z_n ; Local Mass Transfer Products	58
6.2	Effect of Agitation	62
6.3	Effect of Flow	67
6.4	Effect of Plate Spacing	71
6.5	Effect of Phase Inversion and Holdup	72
6.6	Comparison of $\overline{K_o a}$ Observed (This Work) With $\overline{K_o a}$ Predicted	77
6.7	Comparison of $\overline{K_o a}$ Observed (Karr(22)) with $\overline{K_o a}$ Predicted	79
CHAPTER 7	CONCLUSIONS AND RECOMMENDATIONS	84
REFERENCES		87
APPENDIX A	PRESSURE DROP IN A RECIPROCATING PLATE COLUMN	A-1
APPENDIX B	THE EFFECT OF COALESCENCE ON DROPLET BREAKUP	B-1
APPENDIX C	LIST OF TABLES	C-1

LIST OF FIGURES

<u>Figure</u>	<u>Page</u>
1. Karr column (schematic)	10
2. Diagram of plate (actual size)	11
3. Karr column arrangement for the measurement of pressure drop (schematic)	13
4. Karr column arrangement for the sampling and analysis methods (schematic)	14
5. Karr column arrangement for the indicator colour change method (schematic)	15
6. Calibration curve of mercury manometer for water flow rate	17
7. Calibration of rotameter (R1) for water flow rate	18
8. Calibration of rotameter (R2) for kerosene flow rate	19
9. Calibration curve of rotameter (R3) for caustic flow rate	20
10. Calibration curve for the frequency of plate oscillation	21
11. Effect of water flow rate on the time averaged pressure drop in the absence of agitation	28
12. Variation of orifice discharge coefficient with orifice Reynolds number	29
13. Effect of frequency on the time averaged pressure drop	31
14. Comparison of pressure drop with quasi-steady model	34

15.	Equilibrium line in the kerosene-acetic acid-water system at room temperature ($20 \pm 2^{\circ}\text{C}$)	37
16.	Operating and equilibrium lines	39
17.	Material balance in a cocurrent extraction column	39
18.	Neutralization zone (z_n) vs. $-\ln(1-\phi)$	59
19.	Local mass transfer product ($K_o a$) vs. z	61
20.	The analysis of entry effect for ND-10	63
21.	Effect of energy dissipation on $\overline{K_o a}/\epsilon$	65
22.	Effect of agitation on $\overline{K_o a}/\epsilon$	66
23.	Effect of u_o on mass transfer product ($\overline{K_o a}$)	69
24.	Effect of u_o on $\overline{K_o a}/\epsilon$	70
25.	Effect of plate spacing on (H.T.U.)	73
26.	Phase inversion of kerosene-water system (replotted from Ali (1969))	74
27.	Effect of holdup (ϵ) on $\overline{K_o a}$	76
28.	Comparison of $\overline{K_o a}$ observed (this work) with $\overline{K_o a}$ calculated	78
29.	Comparison of $\overline{K_o a}$ observed (Karr data) with $\overline{K_o a}$ calculated	82

List of Tables

<u>Table</u>		<u>Page</u>
1.	Physical properties of materials	C-2
2.	List of valves and pumps, and their use	C-3
3.	Data of the analysis of exit stream	C-4
4.1	Classification of experiments for the indicator colour change method	C-5
4.2	Data of ND-1	C-6
4.3	Data of ND-2	C-6
4.4	Data of ND-3	C-7
4.5	Data of ND-4	C-7
4.6	Data of ND-5	C-8
4.7	Data of ND-6	C-8
4.8	Data of ND-7	C-9
4.9	Data of ND-8	C-9
4.10	Data of ND-9	C-10
4.11	Data of ND-10	C-11
4.12	Data of ND-12	C-12
4.13	Data of ND-13	C-12
4.14	Data of ND-14	C-13
4.15	Data of ND-15	C-13
4.16	Data of ND-16	C-14
4.17	Data of ND-17	C-14

4.18	Data of ND-18	C-15
4.19	Data of ND-20	C-16
5	Cocurrent extraction data for the O-xylene-Acetic acid - water system, obtained by Karr (22)	C-17

8

NOMENCLATURE AND SYMBOLS

A	:	stroke, m extraction factor ($m u_o/u_A$)
a	:	specific interfacial area, $m^2 m^{-3}$
C	:	concentration of solute, $mol m^{-3}$
C_o	:	orifice discharge coefficient
d_p	:	particle diameter, m
d_{32}	:	Sauter mean droplet diameter, m
D_{AB}	:	diffusion coefficient $m^2 s^{-1}$
E	:	stage efficiency
f	:	frequency, Hz
h	:	interplate spacing, m
K	:	overall mass transfer coefficient, $m s^{-1}$
k	:	film mass transfer coefficient, $m s^{-1}$
m	:	distribution coefficient (C_o/C_A)
n	:	number of plates
$\Delta\bar{P}$:	time averaged pressure difference, Pa
Q	:	volumetric flow rate, $m^3 s^{-1}$
Re	:	orifice Reynolds number
S	:	cross-sectional area, m^2
Sc	:	Schmidt number
Sh	:	Sherwood number
u	:	superficial velocity, $m s^{-1}$
u_h	:	the velocity of water through the holes, $m s^{-1}$

- Y : plate displacement, m
 \dot{Y} : plate velocity, $m\ s^{-1}$
 z : total height of plate stack, m
 Z : height of plate stack, m

Greek Letters

- γ : interfacial tension, $N\ m^{-1}$
 ν : kinematic viscosity, $m^2\ s^{-1}$
 ϵ : holdup
 η : column efficiency
 ρ : density, $kg\ m^{-3}$
 σ : fractional open area of plate
 ϕ : parameter (molar ratio of caustic fed in the aqueous phase to acid fed in the organic phase)
 ψ : energy dissipation per unit volume, $W\ m^{-3}$
 ω : angular frequency ($2\pi f$), $m\ s^{-1}$

Subscripts

- A : aqueous phase
 c : continuous phase
 E : entry effect
 n : neutralization
 o : organic phase
 1 : bottom of the plate stack (second subscript)
 2 : top of the plate stack (second subscript)

CHAPTER 1
INTRODUCTION

1.1 Liquid-Liquid Extraction

Liquid-liquid extraction is a separation process that depends on the transfer of the component to be separated from one liquid phase to a second liquid phase that is immiscible or partially miscible with the first. Whether an extraction process is carried out in the laboratory or industry, it always involves contact of the liquid phases with an approach toward equilibrium, and separation of the contacted liquid phases. On the laboratory scale, this is done by shaking the phases in a separatory funnel, leaving them to settle, and then separating the phases. On a large scale, extraction is nearly always carried out continuously, using a variety of equipment designs (1).

The main controlling factors in the transfer rate of the solute(s) are; the area of contact, the mass transfer coefficient and the effective driving force. In the partially analogous case of heat transfer, these factors can be usually evaluated without much difficulty. For example, in a heat exchanger the contact area is merely determined by the geometry of the design, and the heat transfer coefficient in form of Nusselt number is usually known as a

function of Reynolds number and Prandtl number from empirical correlation, while the local effective driving force is the temperature difference which may be easily measured or calculated. In principle, the rate of mass transfer in any extraction device can be calculated in the same way. However, the source of the difficulty lies in the measurement of the three different control factors which can't be easily evaluated in the various types of equipment. For instance, no simple general relation is known between the interfacial contact area and design variables such as throughput of the phases and geometry of distributor and contactor. The contact area depends on fluid-mechanical and interfacial processes which are in most cases too complicated to be analysed from first principles. Similar difficulties are encountered in averaging the local driving force which determines the rate of mass transfer at a given point of the equipment, because in most extraction devices the circulation of the continuous phase results in flow patterns which are neither truly countercurrent nor truly cocurrent.

Despite these difficulties, the three factors controlling the rate of mass transfer, i.e. the contact area, the average driving force and the mass transfer coefficient, are best considered separately assuming that the variables might not be affected by each other.

1.2 Characteristics of the Karr Reciprocating Plate

Column

A reciprocating plate extraction column having only 10% of open area was first proposed by Van Dijck in 1935 (2). In contrast, the reciprocating plate column introduced by Karr in 1959 (3) has a relatively large fractional open plate area in the order of 60%. This characteristic permits a relatively high throughput per unit area even without a serious loss of efficiency, coupled with ease of plate removal and cleaning. The uniform power dissipation over the cross-sectional area of the column also provides relatively uniform droplets (for example, compared with the rotating disc contactor) and negligible channelling effect. Thus the H.T.U. (Height of a Transfer Unit) and flow capacity are nearly independent of column diameter. Since this makes the scale up of Karr column straightforward (4) and provides several advantages over other extraction devices, Karr columns are now widely used industrially in sizes up to 1.0 m in diameter.

The mass transfer performance and the hydrodynamic characteristics of Karr type of reciprocating plate column have been extensively investigated since its introduction in 1959.

The studies on mass transfer performance parameters such as H.E.T.S., H.T.U. and column efficiency have been

carried out by Karr and others (3,5,6). Hydrodynamic characteristics such as the size of droplet, holdup, axial dispersion, power consumption, and flooding have been extensively studied by Baird and others (7-11,36). In order to simulate the overall mass transfer performance in the reciprocating plate column, a design model which combines the basic correlations and theory on the reciprocating plate column has been developed (12). Such a model allows designs to be carried out with confidence for systems which have not previously been handled.

1.3 Mass Transfer with Instantaneous Chemical Reaction

Liquid-liquid extraction accompanied by a homogeneous chemical reaction in one phase has been carried out industrially for many decades (e.g. nitration, sulphonation, alkylation, etc.). As the nuclear industry and other hydrometallurgical extraction processes have been rapidly developed, a large new industrial class of organometallic reactions has appeared.

In mass transfer with instantaneous reaction, the chemical reaction occurs in an infinitesimally thin reaction zone, near (but not at) the interface. The concentrations of both reactants tend to be zero at this zone and the mass transfer rate is controlled only by the diffusion of reactants to the zone. This effect is well understood in

connection with enhanced absorption and extraction, as summarized by Astarita (13) and Danckwerts (14).

Other applications of mass transfer with instantaneous reaction can involve direct flow visualization, for example, sodium hydroxide solution with phenolphthalein has been injected into dilute hydrochloric acid solution to study vortex rings (15) and batch mixing (16), and in the visual measurement of axial dispersion coefficients (9). These flow visualization applications have recently been reviewed by Baird (17).

The indicator colour change visualization technique has been developed in this work (see Section 4.3) to measure the volumetric mass transfer coefficient for a 5.08 cm I.D. Karr column in cocurrent extraction. A dilute solution of acetic acid in kerosene was dispersed in the dilute aqueous solution of sodium hydroxide in the Karr reciprocating plate extraction column. It was assumed that the acetic acid transfer resistance would mainly lie in the organic (dispersed) phase due to the very small distribution coefficient of acetic acid between water and kerosene (see Section 4.1). The acetic acid transferred from the organic droplets reacts instantaneously with the aqueous caustic in the presence of an indicator (phenolphthalein) and this too drives the controlling resistance towards the organic phase. In the aqueous phase, free sodium hydroxide is present up to

a certain level in the column which is indicated by the sharp change of colour from red to white in the presence of phenolphthalein. This boundary takes up a position in the column depending on the operating conditions such as flow rates, agitation intensity, or concentrated caustic injection rates. The mass transfer rate was measured by reading the neutralization boundary at various conditions. This technique is considered to be much better than sampling and analysis of exit streams, which tend to undergo mass transfer during the sampling procedure.

1.4 Karr Reciprocating Plate Extraction Column as a Cocurrent Contactor

Multiple mixers in series for use in mixer-settler extraction systems offer some advantages such as improving mixer efficiency, and reduced settler volume (18-21). This suggests the employment of a cocurrent plug flow contactor. Nearly all the work to date on the characteristics of Karr type of reciprocating plate column has involved counter-current operation. In this work, the Karr reciprocating column has been employed as a cocurrent contactor which gives several benefits such as high throughput, flexibility of operation, a close approach to isotropic turbulence, and possibly small settler volume. Since there is no limitation of flow rate by flooding and agitation, very high

throughputs per unit column area can be employed. Superficial velocities of fluid in the order of 10 cm/s have been studied in this work. It will be shown that it is reasonable to assume the plug flow in the column at these velocities. The sizes of droplets being created by pulsation are relatively uniform due to the uniform agitation over the cross-sectional area of the column (8) so that the formation of emulsions can be easily prevented by controlling the intensity of agitation or flow rate. Some earlier experimental results obtained by Karr for the low interfacial tension systems indicated the need to optimize the agitation intensity. Excessive agitation might result in prolonged settling time, and therefore, large settler volumes (22).

Measurement of mass transfer rate has been carried out both by the indicator colour change method and the sampling and analysis of exit streams. The data obtained by the indicator colour change method have been compared with the model combining a specific surface area and overall mass transfer coefficient.

Some of the data of Karr, who performed cocurrent extractions of acetic acid in o-xylene - water system (water dispersed) in a 2.54 cm I.D. Karr column (22), have been compared with a model in which Levins' mass transfer coefficient correlation was employed.

The overall objective of this work is to arrive at and confirm experimentally a model for cocurrent mass transfer in reciprocating columns, using some of the same methods that have proven useful in the development of a countercurrent mass transfer model (12).



CHAPTER 2

APPARATUS DESIGN AND EXPERIMENTS

2.1 Equipment Design and Calibration

A Karr reciprocating plate column, shown schematically in Fig. 1, was constructed of six flanged glass sections and two stainless steel sections at top and bottom. The bottom stainless steel section has two 1.9 cm I.D. nipples for the inlet of the organic phase and the aqueous phase, and one 0.63 cm I.D. nipple for the manometer arrangement, and a central baffle between the two phase inlets, as shown. The bottom plate of the column was provided with a drain. There is a 4.7 cm I.D. overflow for the outlet of fluid in the top stainless steel section, with the top of the column open to atmosphere.

The overall height of the column is 2.4 m. The plate stack is 1.46 m in height and is mounted on a stainless steel reciprocating drive shaft. Perforated stainless steel plates having 61% open area and 13.7 mm diameter perforations were spaced at uniform intervals on the shaft. A diagram of the plate is illustrated at Fig. 2.

Reciprocation was provided by an electric motor and speed controller (3/4 hp., 0-400 r.p.m., respectively) at the top of the column which drive an adjustable crankshaft

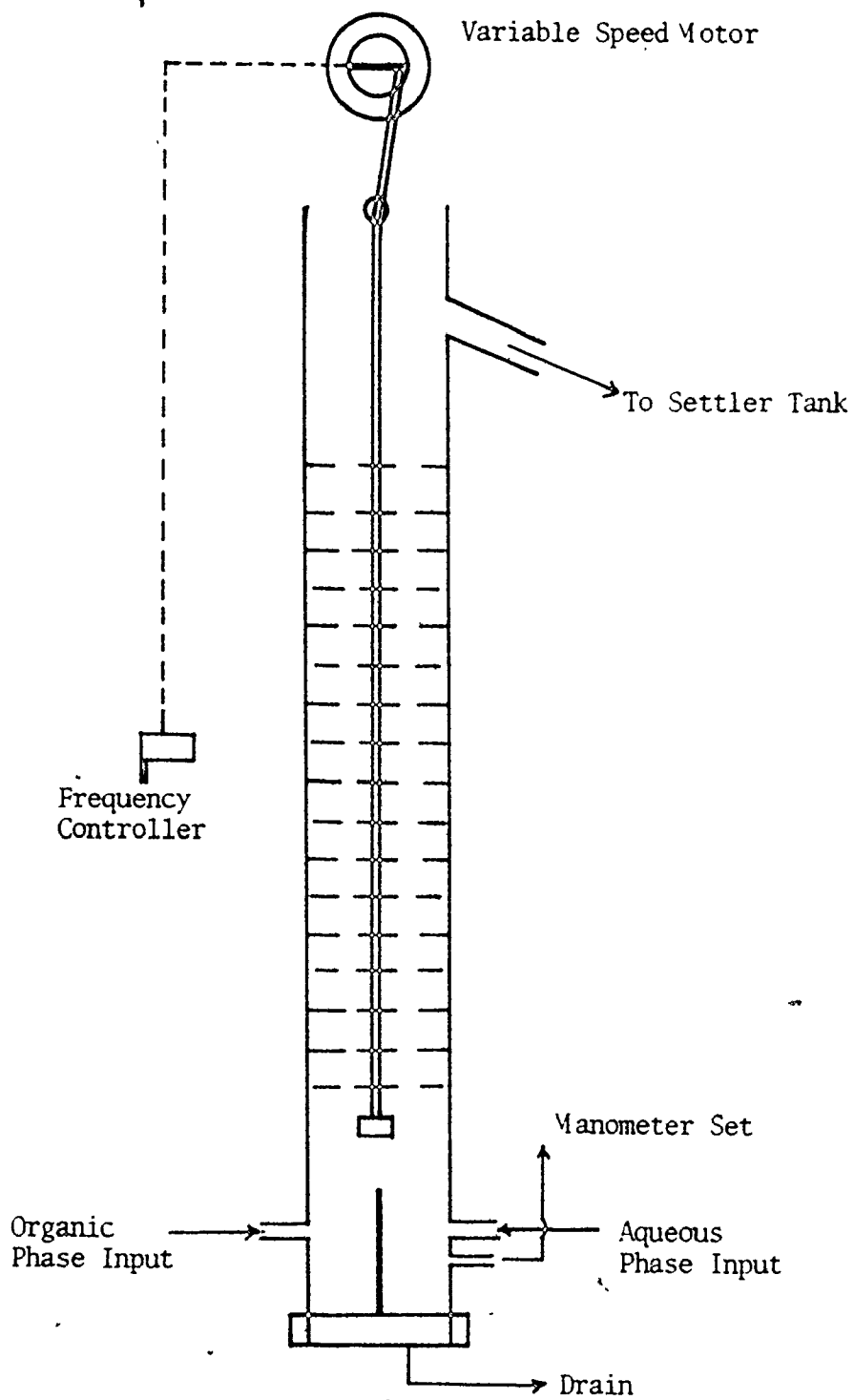


Figure 1. Karr column (schematic)

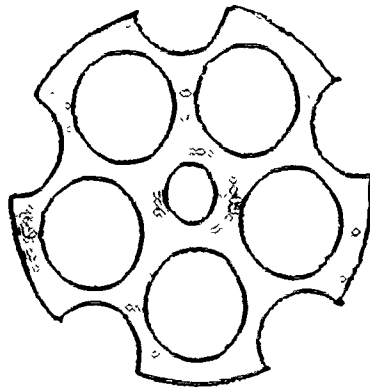


Figure 2. Diagram of plate (actual size)

assembly (0-4.5 cm stroke) connected to the agitator shaft. The frequency of reciprocation has been varied up to 6.0 Hz with a constant stroke of 4.5 cm.

Three different arrangements of input lines have been employed as shown in Figures 3 to 5.

For the measurement of pressure drop in single phase flow (Fig. 3), a simple manometer set was connected to the bottom nipple of the column. The water was supplied through 1.9 cm I.D. copper tube and 1.9 cm I.D. Tygon tube from the public tap water line (approximately 10°C) and the flow rate was measured by an orifice-mercury arrangement which has a restriction in the line to reduce the pressure fluctuation effects due to the pulsation of the plates.

For the mass transfer measurement by the sampling and analysis of exit streams (Fig. 4), the water was provided through the same line as used in the pressure measurement. A rotameter (R1) was installed and the water flow rate has been controlled by the valve (W2). The organic phase was fed from an 180 L top reservoir (T1) through 1.3 cm I.D. PVC pipes via a centrifugal pump (P1). The organic flow rate was measured by a calibrated rotameter (R2) and a gate valve (W2). Some Tygon tubing connections, as shown in Fig. 4, were made for operational purposes.

A slight modification in the water supply lines was made for the indicator colour change technique. Two

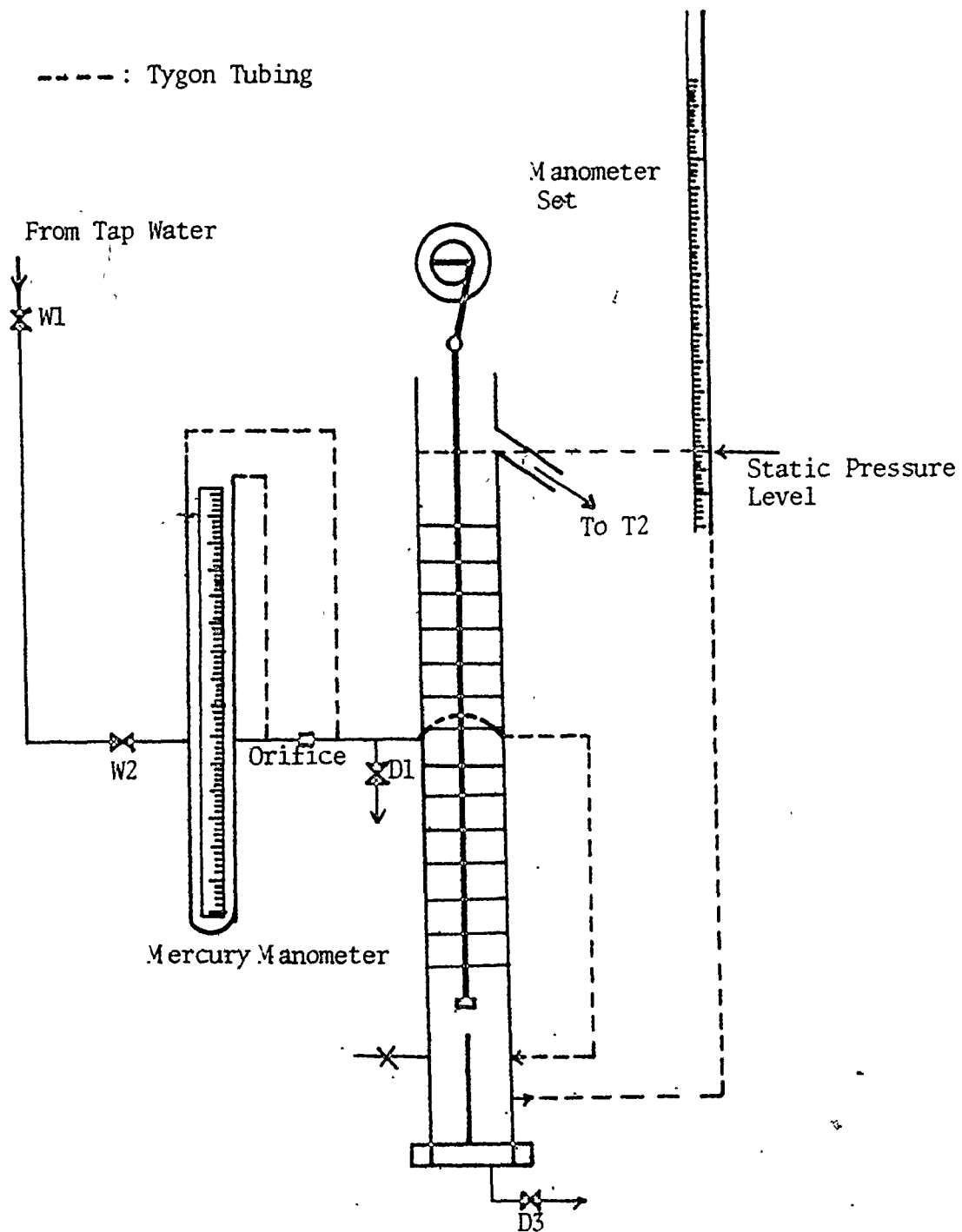


Figure 3. Karr column arrangement for the measurement of pressure drop
(schematic)

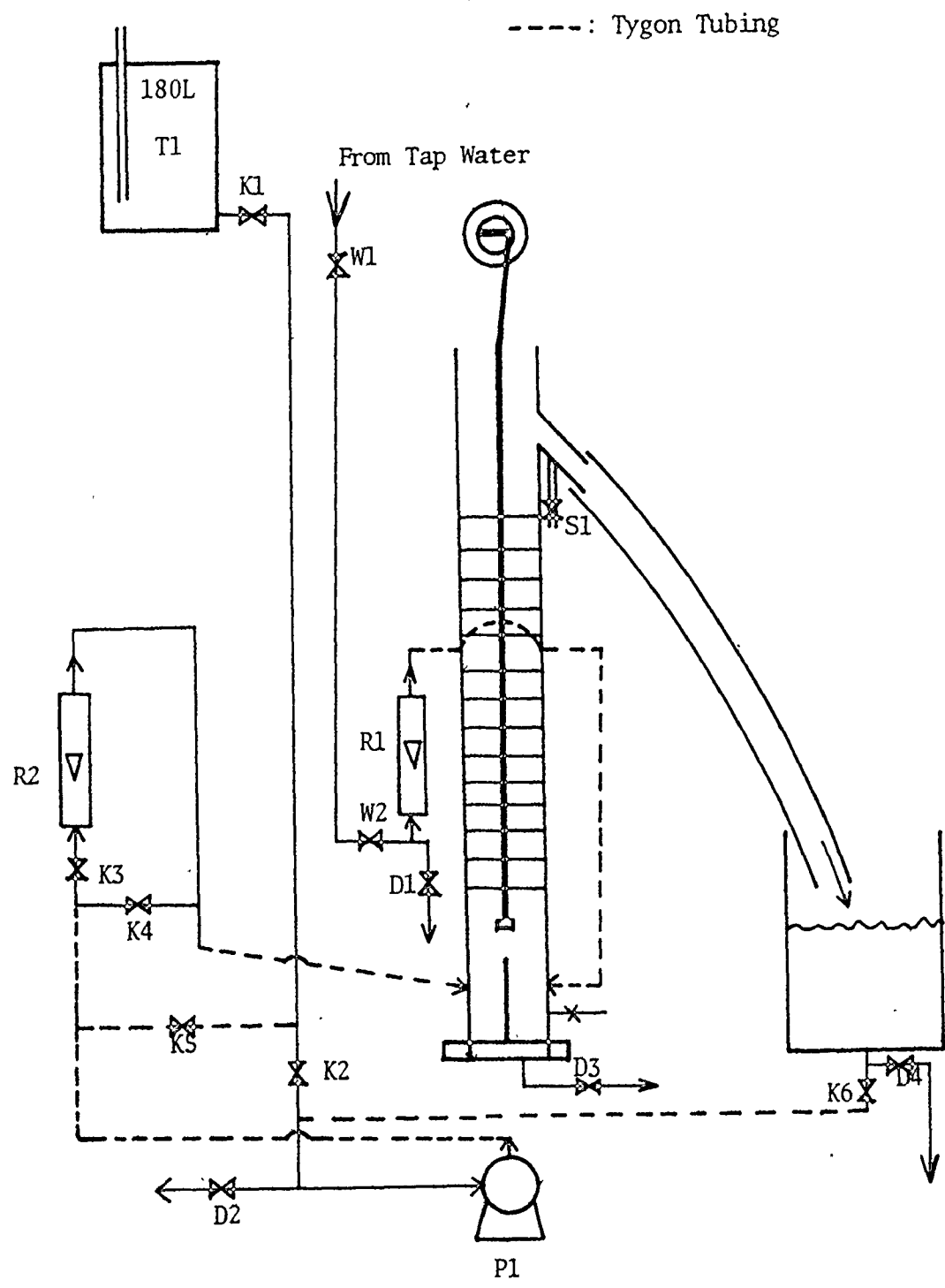


Figure 4. Karr column arrangement for the sampling and analysis method (schematic)

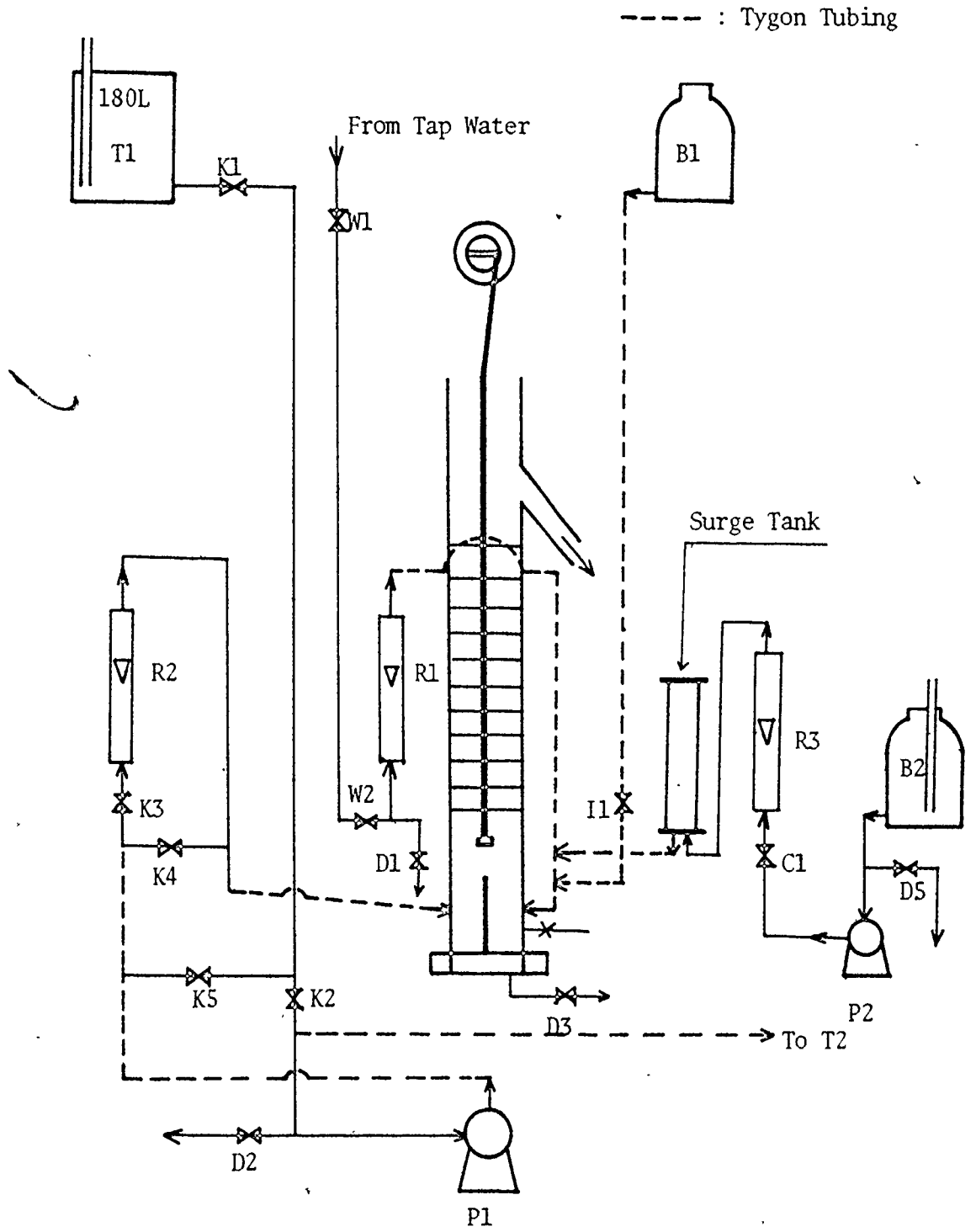


Figure 5. Karr column arrangement for the indicator colour change method (schematic)

injection lines were connected to the water line as shown in Fig. 5. Indicator solution was injected from a 20L overhead bottle (B1) through 0.64 cm I.D. Tygon tubing and the flow rate was controlled by a needle valve (I1). Concentrated caustic solution in a 20L bottle (B2) was pumped by a centrifugal pump (P2) through 1.3 cm I.D. stainless tubing via a surge tank which reduces the effect of pulsation of plate on the caustic flow rate. A calibrated rotameter (R3) and a stainless steel needle valve (C1) were installed for the measurement of caustic flow.

Bubblers were provided in the kerosene storage tank (T1) and the caustic storage bottle (B2) in order to remove the effect of liquid level in the vessels upon flow rates.

The rotameters were carefully calibrated and the accuracy in the flow measurement was approximately $\pm 2\%$. The frequency of plate reciprocation was calibrated both by a stroboscope and by counting the movements of the shaft at the intervals of two minutes. The calibration curves for the rotameters, the mercury manometer, and the frequency are given in Figures 6 to 10.

2.2 Preparation and Analysis of Materials

In view of the size of the column and the high flow rates, it was not practicable to take special precautions on the purity of the liquids, therefore tap water and

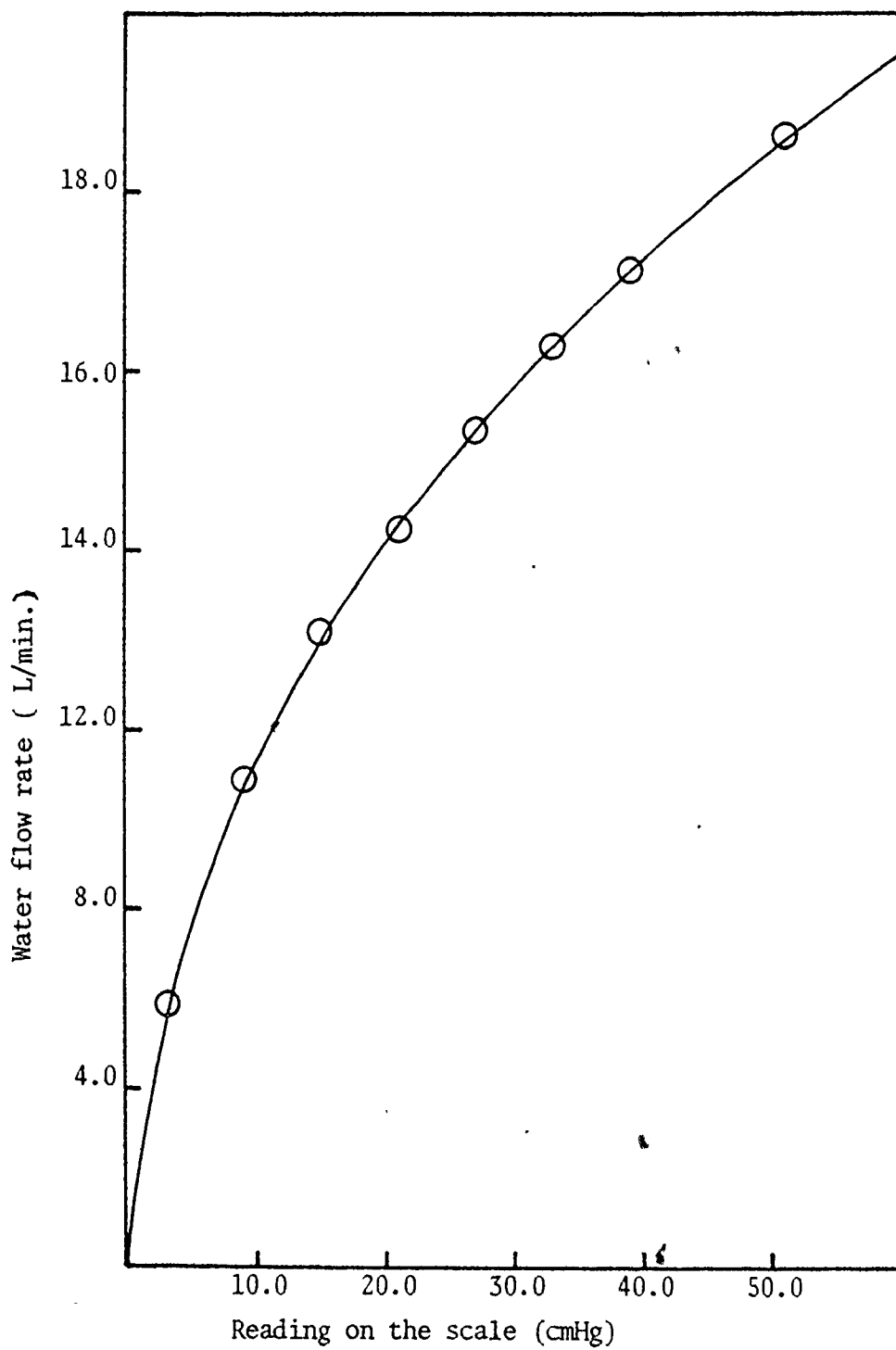


Figure 6. Calibration curve of mercury manometer for water flow rate

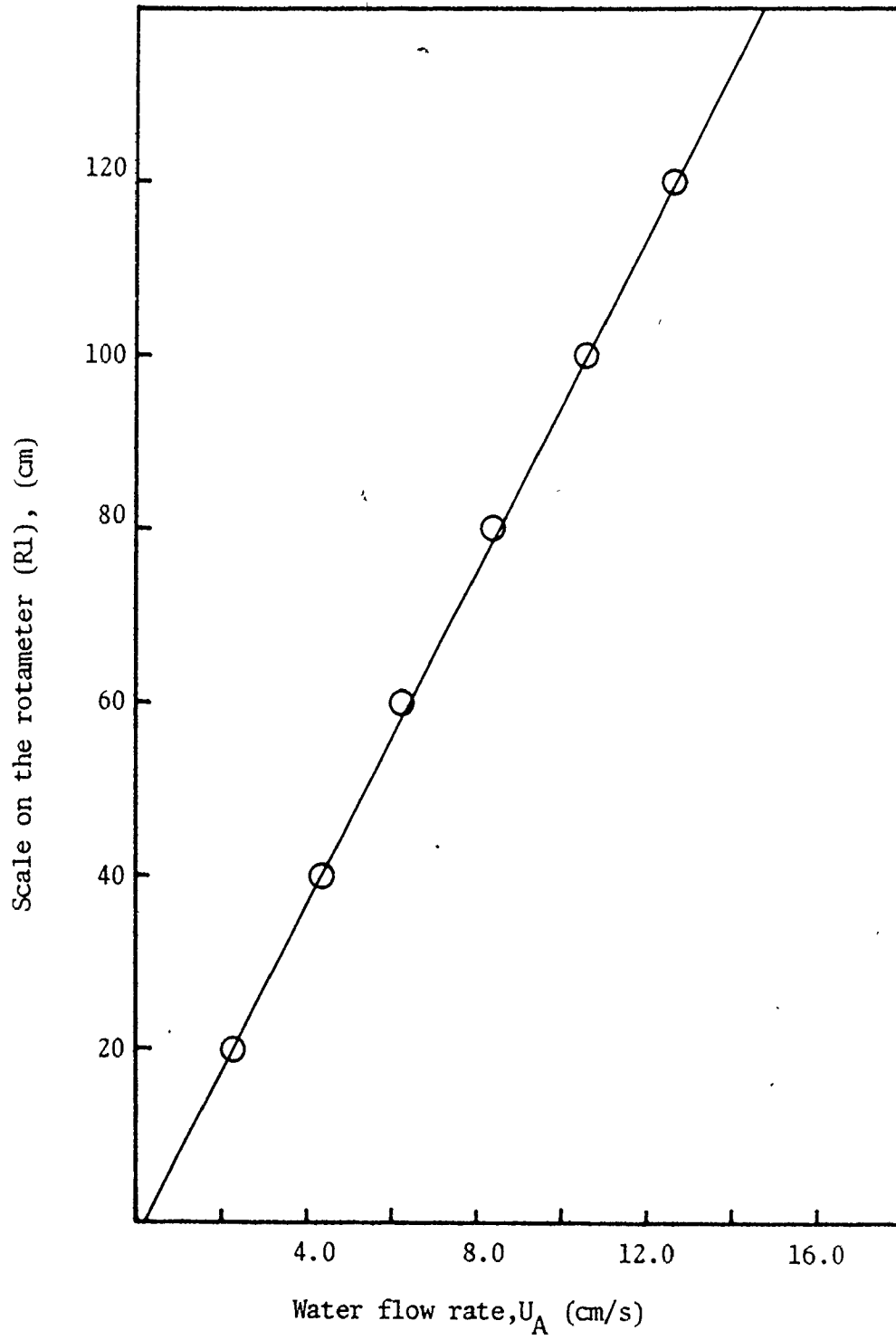


Figure 7. Calibration of rotameter (R1) for water flow rate

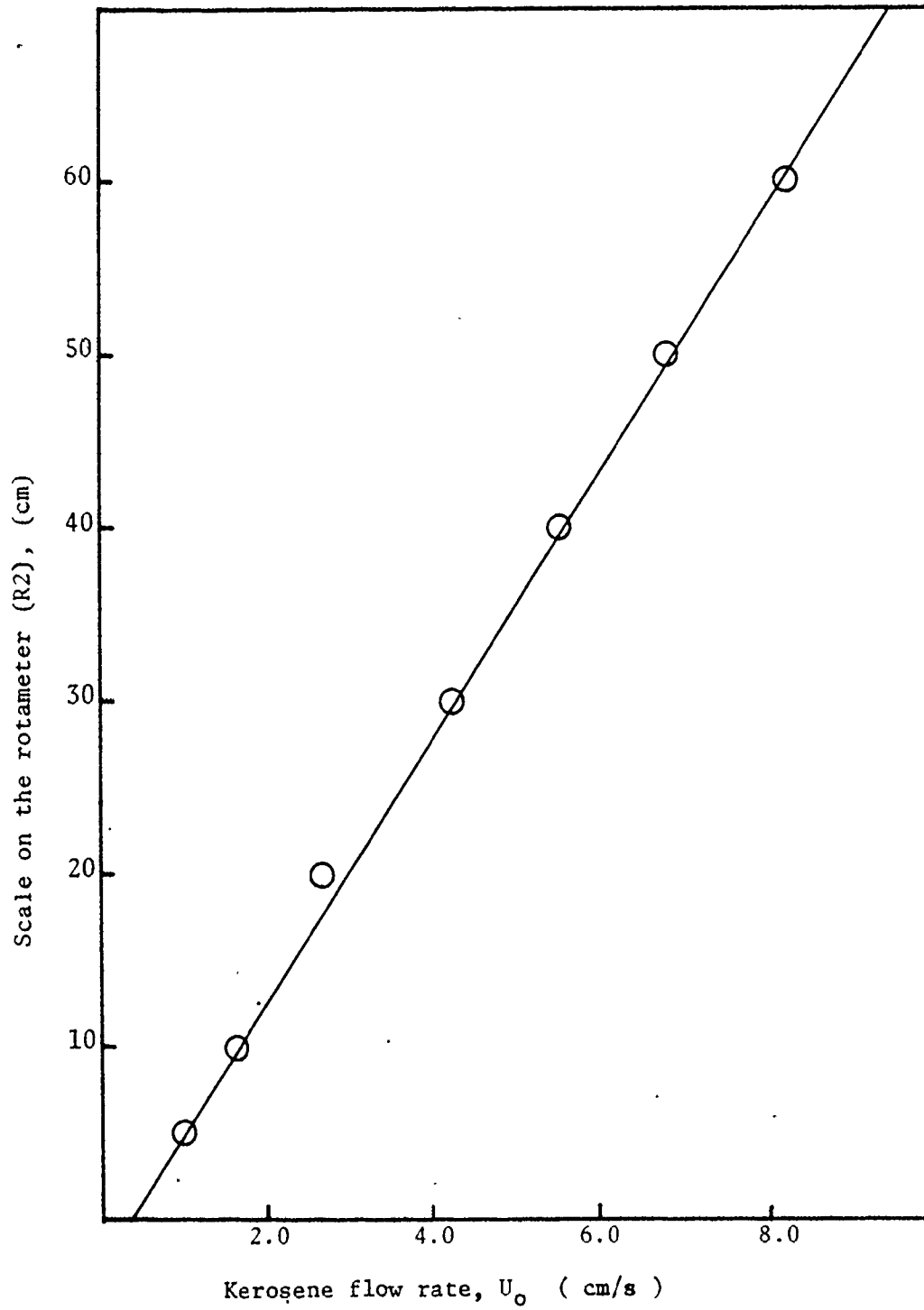


Figure 8. Calibration of rotameter (R2) for kerosene flow rate

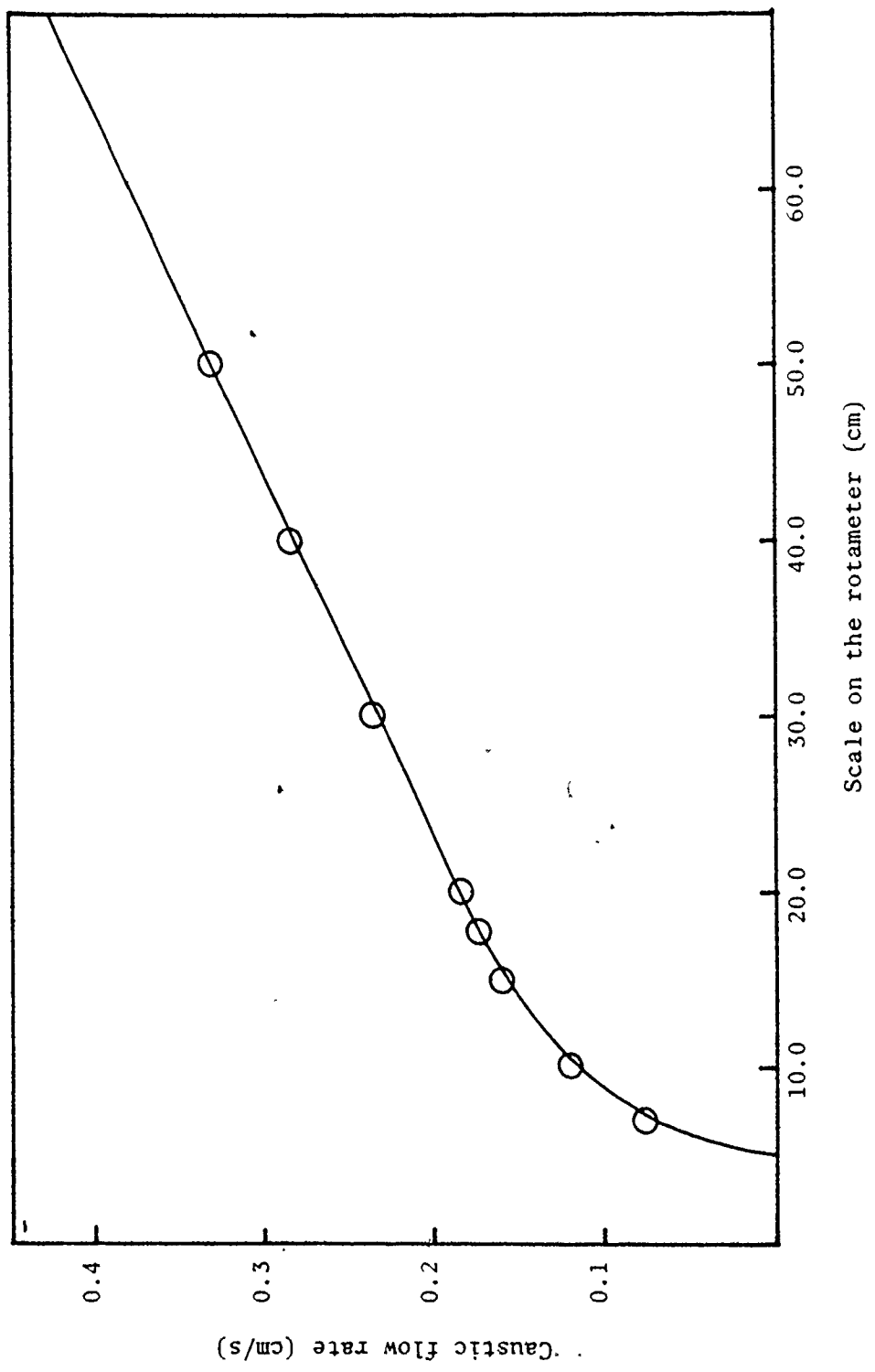


Figure 9. Calibration curve of rotameter (R3) for caustic flow rate

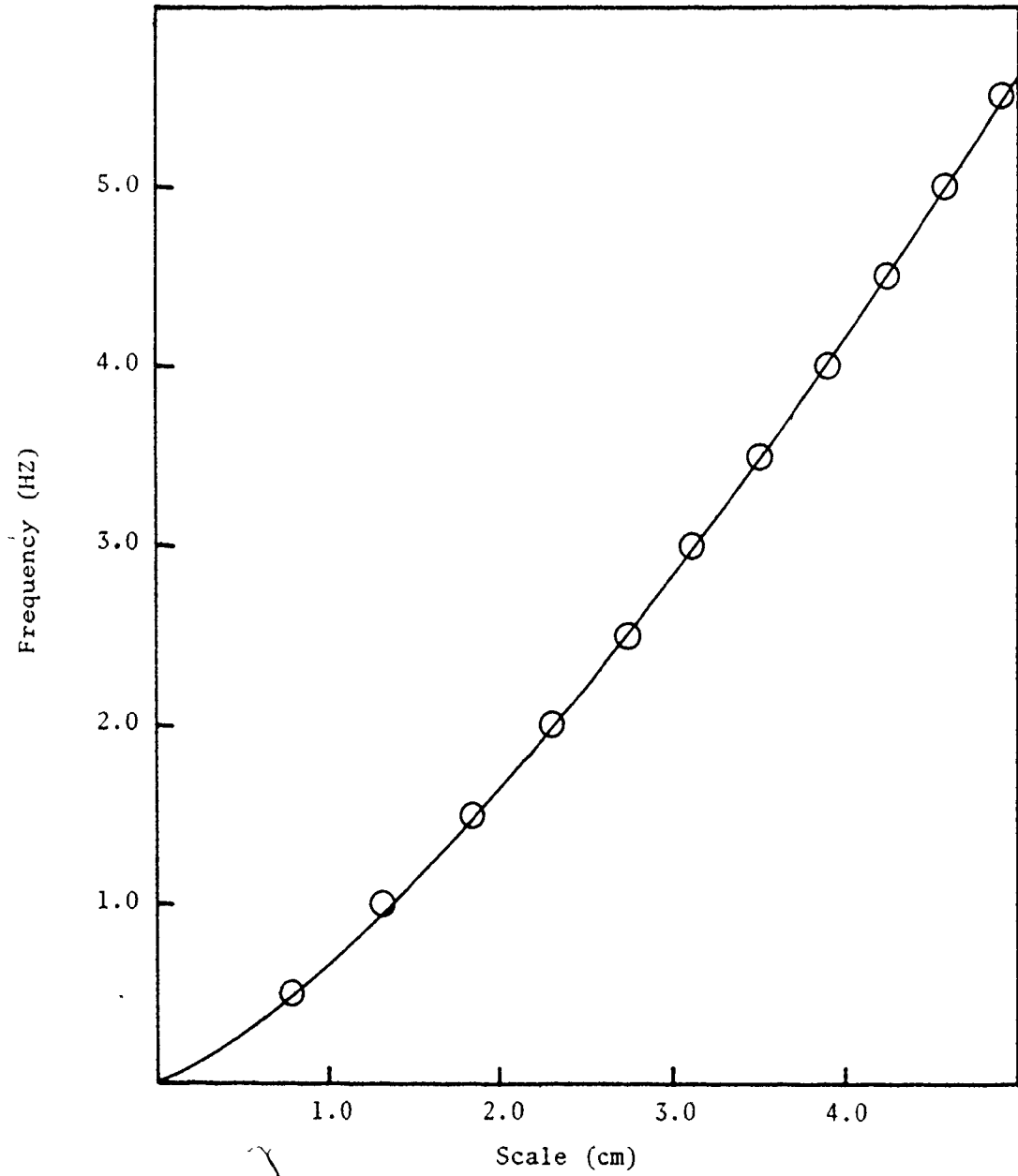


Figure 10. Calibration curve for the frequency of plate oscillation

commercial kerosene (see properties in Table 1, Appendix C) were used throughout. Kerosene and water were mixed through the column under high agitation so that the kerosene was presaturated with water before use. Low concentration of acetic acid in kerosene (approximately 1-2%) was made up by adding glacial acetic acid to the kerosene in the tank and then mixing it through the column at high agitation in the absence of an aqueous phase until a homogeneous organic phase could be obtained. The prepared organic phase was pumped to the top reservoir (T1) and then sampled for analysis just before its use. The concentration of acid in the organic phase was purposely not varied greatly in order to minimize the effect of solute concentration on the results.

20 mL of the organic phase was sampled from the top reservoir just before each run and then added to 100 mL of distilled water in a 250 mL separatory funnel, which was then vigorously shaken for 3-5 minutes. The aqueous phase was removed after the two phases were completely separated. Then it was titrated with standard sodium hydroxide solution. Due to the very small distribution coefficient of acetic acid between water and kerosene (to be discussed in Section 4.1), it was assumed that most of acid would be transferred to the excess water. The concentration of sodium hydroxide solution used was determined by titration

with standard hydrochloric acid prepared from ampoules.

For the indicator colour change method, a stock solution of sodium hydroxide was required. This was made up in approximately 1.0 mol/L strength from AR grade pellets and distilled water. The exact strength was determined by titration with standard hydrochloric acid. Phenolphthalein indicator solution was prepared as a 0.1% solution of solid phenolphthalein in 40% water and 60% ethanol.

2.3 Operating Procedures

For the sampling and analysis of exit streams, about 180 L of the organic phase was prepared in the top reservoir (T1) before each run. The water flow was first started through the column at a given plate oscillation frequency for about 5 minutes in order to wash out the column and the tubing and was then set by the valve (W2). The organic phase was then fed via the pump (P1) and the flow rate was set by the valve (K3) while the other valves (K4, K5) were closed. After steady state condition was obtained in most of runs within two minutes due to the high flow rate and relatively uniform energy dissipation along the column, the readings of rotameters (R1, R2) were recorded and then a sample was taken from the overflow line (S1) in a 250 mL separatory funnel and the phases were separated as quickly as possible. Because of high interfacial tension between

kerosene and water, this separation was completed within 30 seconds in most runs. The separated phases were titrated by standard sodium hydroxide. Special caution was needed for analysis of the organic phase due to its low concentration, as will be discussed in Section 4.2.

The operating conditions such as flow rates and agitation intensity were varied in each new run, with the overflow being taken approximately two minutes after the operating conditions had been set.

For the indicator colour change method, the water flow was started and the agitation frequency was set, then the concentrated caustic solution was injected by the pump (P2) into the water stream at constant flow rate. Indicator was then added at a steady flow of about 0.2 mL/s, resulting in the red colour of the aqueous phase throughout the column. Then the organic phase flow was started. Since the acid transferred from the dispersed organic droplets reacted instantaneously with the dilute aqueous caustic solution, a sharp colour boundary within the plate stack was observed. At this point, the moles of acid transferred per litre of the aqueous phase exactly balanced the initial aqueous caustic concentration. The colour boundary reached a steady position within one minute in most experiments. The readings of rotameters (R1, R2, R3) and the height of the colour boundary were recorded.

The neutralization zone has been varied by changing one of the following conditions while others were kept uniform; the concentrated caustic flow rate, the water flow rate, the organic phase flow rate, or frequency of agitation.

A floodlight and white background were used to facilitate observation of the colour boundary. The accuracy in the observation of neutralization zone was approximately less than ± 2.0 cm in most runs. Temperature of the fluid in the column was about $10 \pm 1^\circ\text{C}$ in all runs. After each set of experiments, the column and the tubing were washed out by running tap water. Table 2 (Appendix C) lists the valves and their uses.

CHAPTER 3

PRESSURE DROP IN THE KARR COLUMN

An important practical consideration in cocurrent flow at high throughputs, is the frictional pressure drop. This will have a bearing on the cost of pumping equipment required and therefore the total cost of a cocurrent mass transfer device. In this work, only single phase (aqueous) flow is considered. It is anticipated that the pressure drop in two phase cocurrent flow in the emulsion regime would differ from the single phase values only to the extent that the dispersion density is different.

A simple manometer set, as shown in Fig. 3, was installed to measure pressure difference. The column was initially filled with water and the static pressure difference between the inlet and the outlet of the column was recorded. A series of experiments have been carried out under the following conditions and the pressure deviation from the static pressure was observed.

- i) single phase flow without agitation
- ii) plate oscillation in the absence of flow
- iii) single phase flow with agitation

Accuracy in the measurement of pressure drop was

approximately $\pm 5\%$. The experimental results were compared with the values predicted from the model presented in Appendix A.

Case i) Single phase flow without agitation

The water flow rate was varied and the observed pressure drop has been plotted against the water velocity (U_c) as shown in Fig. 11. The predicted values appear higher at high velocity while at low velocity, predicted values are less than observed data. This might be due to the variation of the orifice discharge coefficient (C_o) with the orifice Reynolds number of the system. However, it was assumed that the discharge coefficient was constant ($C_o = 0.60$) in the derivation of the model. In a normal orifice, the discharge coefficient approaches 0.60 only at high Reynolds numbers (23). The variation of C_o with Re in the present column was calculated from the data and equation A-4 and is represented in Fig. 12 which shows the same type of curve as a standard orifice. This curve is not identical because of the difference in geometry between a multiply perforated plate and a single standard orifice.

Case ii) Plate oscillation in the absence of flow

In this run, water was first filled up to approximately 5.0 cm below the outlet of the column so that

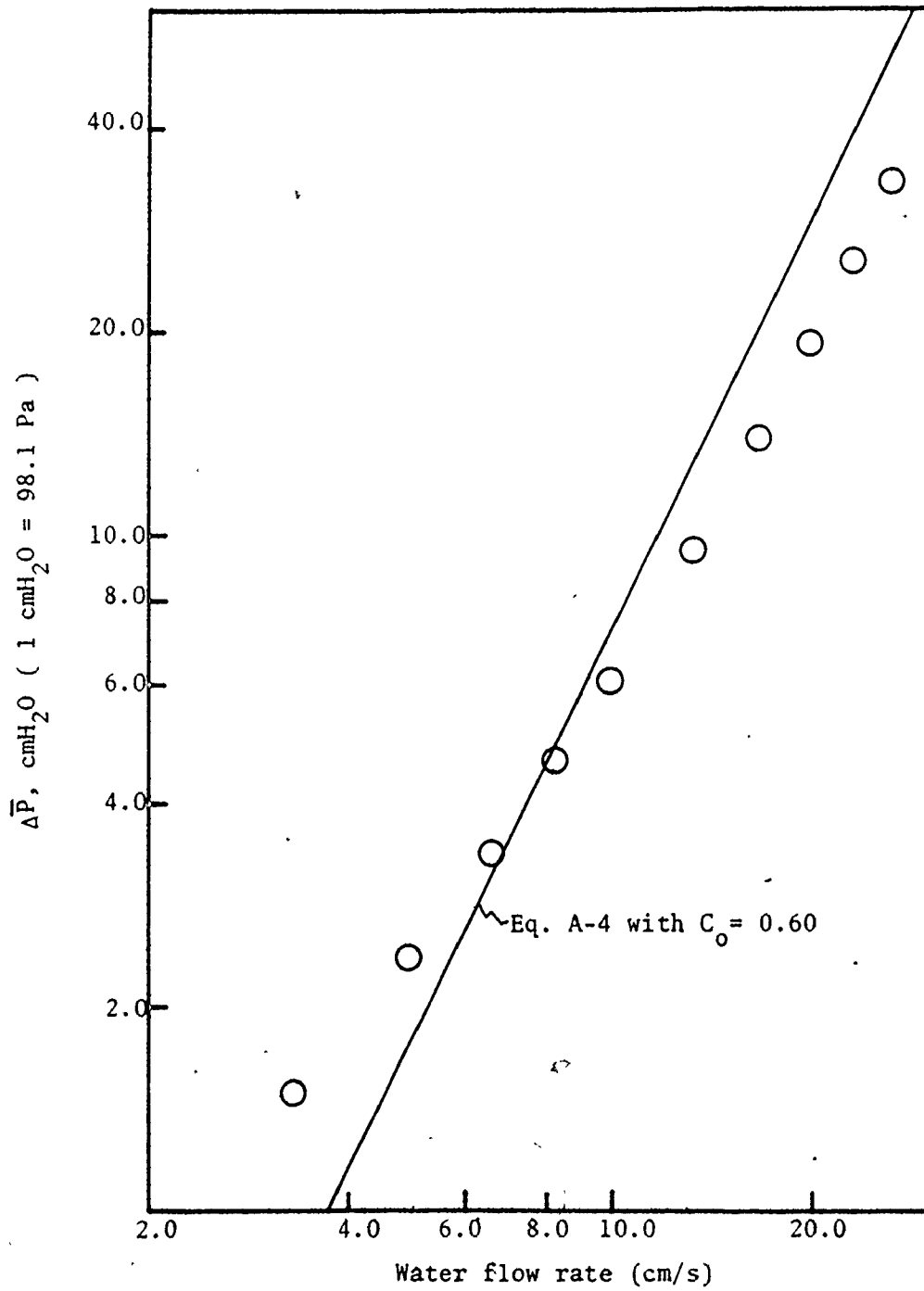


Figure 11. Effect of water flow rate on the time averaged pressure drop in the absence of agitation.

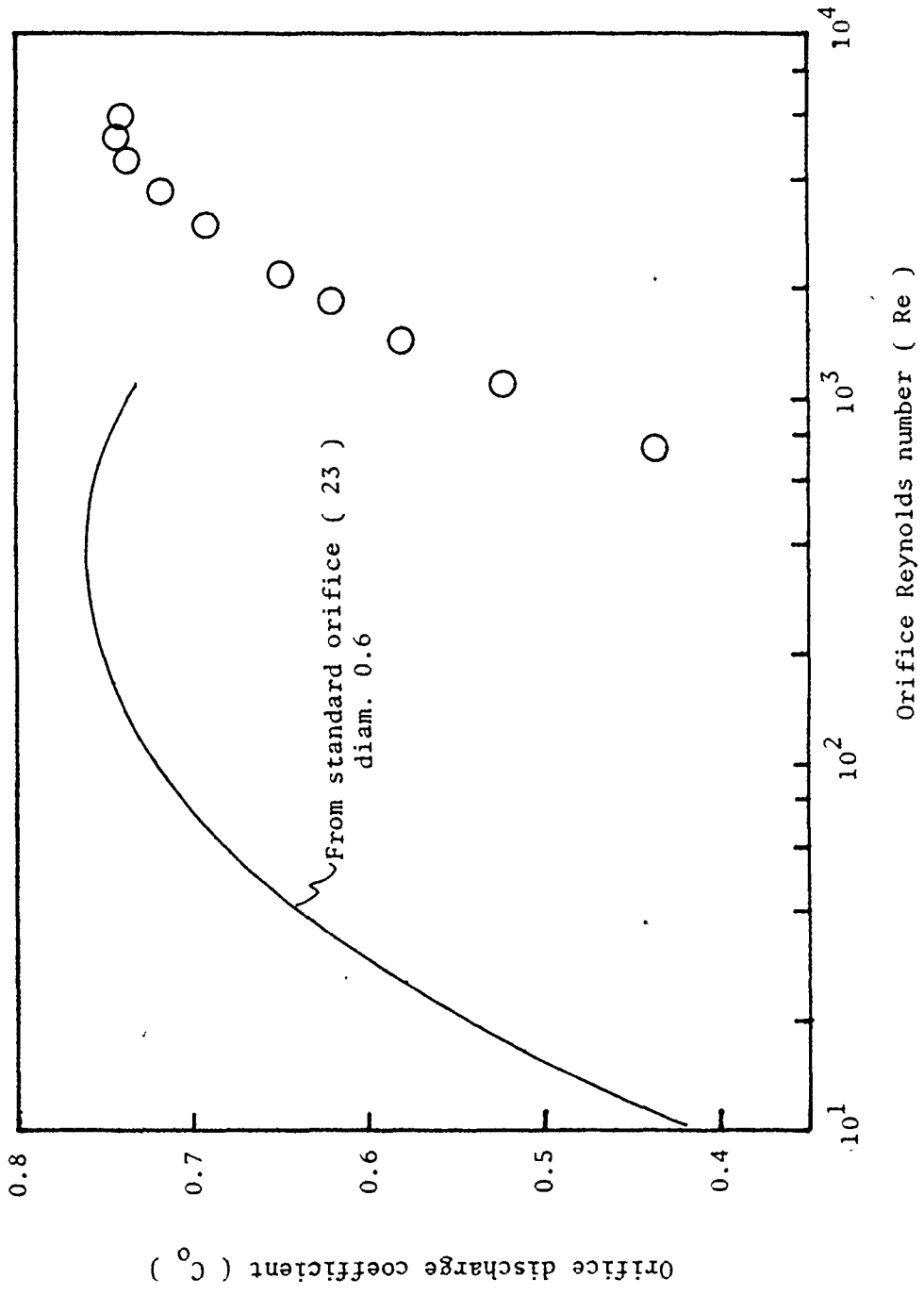


Figure 12. Variation of orifice discharge coefficient with orifice Reynolds number.

overflow of water due to pulsation could be prevented. The static pressure level was checked before and after each run. The frequency was varied from 0.5 Hz to 6.0 Hz at constant amplitude (2.25 cm). The pressure difference from the static pressure was measured and plotted as a function of frequency as shown near the bottom of Fig. 13. According to the theoretical model given in Appendix A, the time averaged pressure difference should be zero because of the symmetrical movement of the plate. However, measured $\Delta\bar{p}$ tends to increase up to 3.0 cm H₂O at 3.5 Hz and then decreases, as the frequency is increased further. This result might be explained as follows; the Tygon tubing of the water inlet line (19.0 mm I.D.) might be partially collapsed when the pressure drops below atmospheric pressure, i.e. when the plate stack has its maximum upward velocity. Thus at $f=3.5$ Hz, the minimum pressure calculated from equation A-8 is about 99.7 KPa. Contraction of the tube may result in an increase in the average pressure because of a raising of the "trough" of the pressure wave-form due to this effect. This hypothesis is also consistent with the maximum in the observed $\Delta\bar{p}$ curve (Fig. 13) because at very high frequencies the tube walls would not have time to deform.

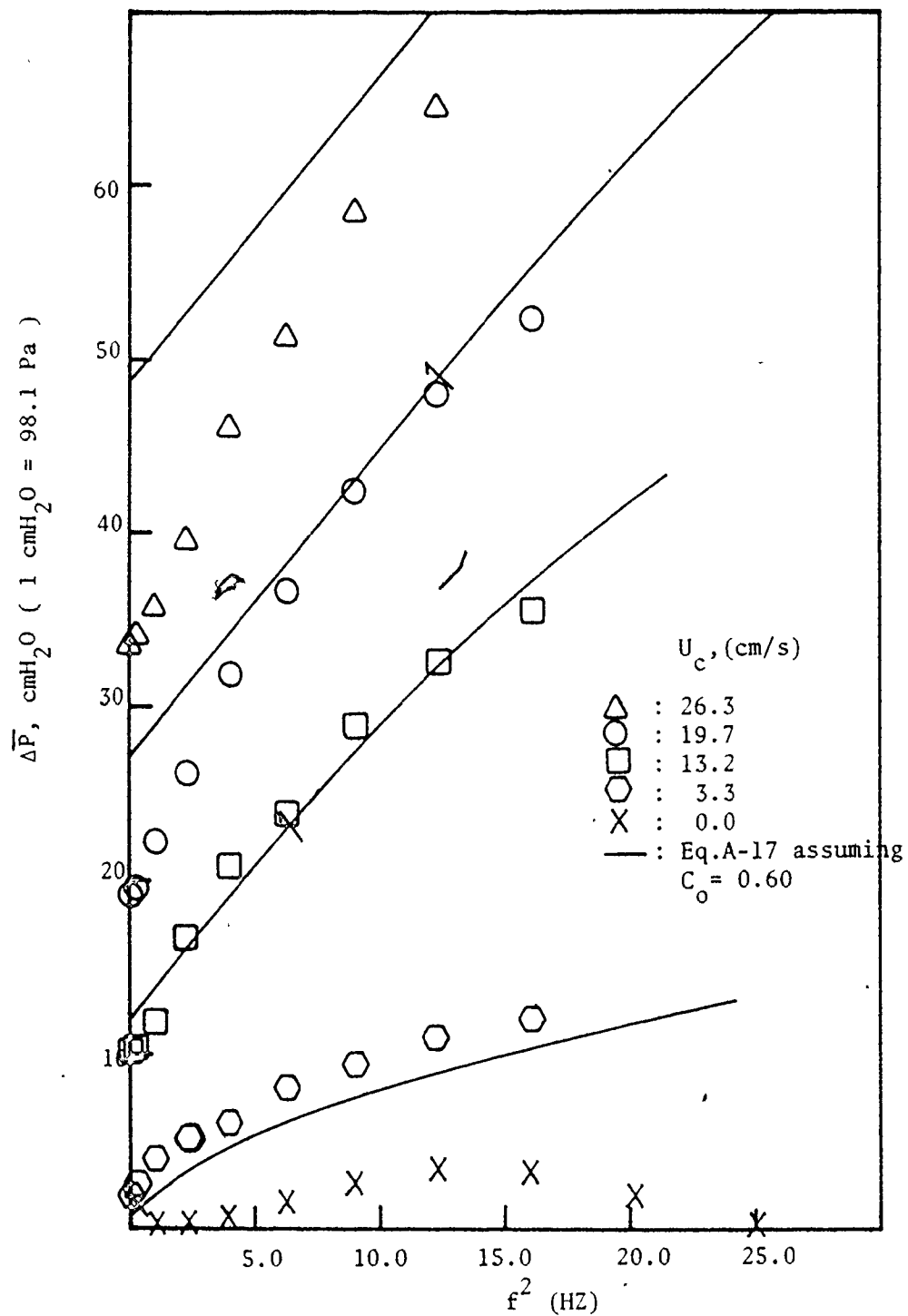


Figure 13. Effect of frequency on the time averaged pressure drop

Case iii) Single phase flow with agitation

The last series of experiments have been performed with variation of both frequency and water flow rate. This series is of course the most relevant to practice. The superficial velocity of water has been varied up to 26.0 cm/s and the frequency up to 6.0 Hz with constant amplitude. Some typical data are presented in Fig. 13. The continuous curves are obtained from equation A-17 assuming $C_o = 0.60$. At the lowest flow rate investigated, the data lie consistently above the prediction; this could be due to the same effect of partial collapse of the inlet tubing as noted previously. This effect would be less important at higher flow rates, as the pressure at the base of the column would never fall much below atmospheric.

As the flow rates are increased, the data points tend to fall below prediction, particularly at low agitation frequencies. This deviation is in the same direction as noted for steady flow (Fig. 11) and can be explained in terms of a higher effective orific coefficient C_o than the assumed value of 0.60. The flow through the perforations at low frequencies is always unidirectional, but flow reversal begins to occur when the parameter V (see Appendix A) exceeds unity; the frequencies at which this occurs are shown as arrows on the curves in Fig. 13. It will be seen that the deviation of C_o from 0.60 tends to lessen

considerably as flow reversal takes place.

An alternative data presentation is shown in Fig. 14, with $\Delta\bar{p}$ plotted against the right hand side of equation A-17. The overall average C_o found by regression analysis of this plot is 0.64.

It may be concluded from this section that the time-averaged pressure drop is substantially increased by increasing reciprocation frequency at a given flow rate. The effects of flow and frequency are approximately predictable from the quasi-steady equation developed in Appendix A, but the accuracy of prediction is somewhat limited by the variations in effective orifice coefficient C_o .

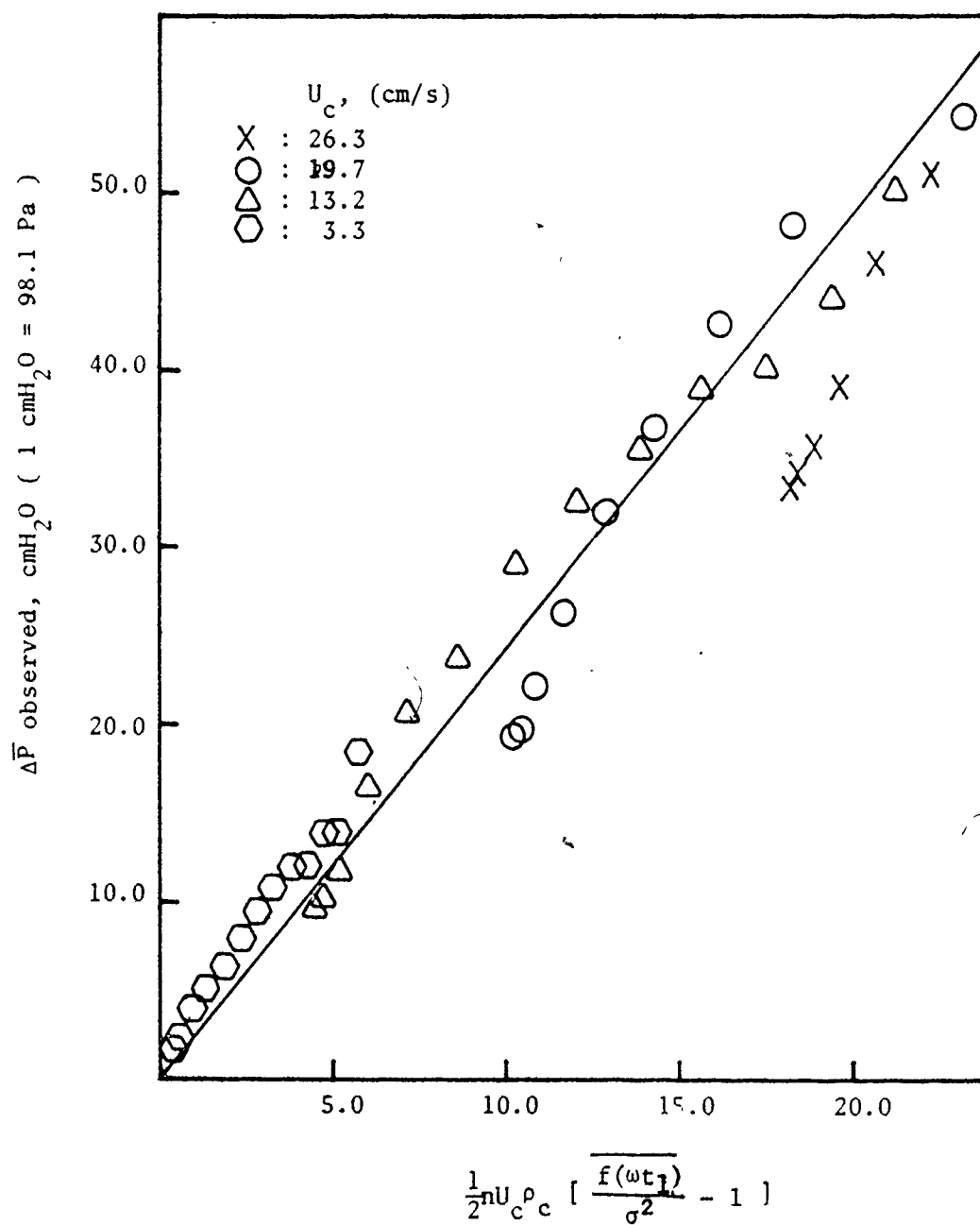


Figure 14. Comparison of pressure drop with quasi-steady model.

CHAPTER 4
MASS TRANSFER MEASUREMENT

4.1 Operating and Equilibrium Lines

If a liquid solvent is added to a solution of some solute in a second solvent, either immiscible or only partially miscible with that which is added, then the solute will distribute between the two liquid phases until equilibrium is established. The solute's concentrations in the two phases at equilibrium will depend on its relative affinities for the two solvents. The ratio of the concentrations of solute in the two phases at equilibrium is called a distribution coefficient, m , and gives a measure of the relative affinity of the solute for the two phases.

$$m = \frac{C_o}{C_A}$$

where C_A ; conc. of solute in aqueous phase

C_o ; conc. of solute in organic phase.

For measurement of distribution coefficient of acetic acid in the kerosene-acetic acid-water system, glacial acetic acid solution was weighed and then added to 50 mL of kerosene presaturated with water in a 250 mL separatory funnel. A homogeneous kerosene mixture was obtained after

3-5 minutes shaking and then 50 mL of tap water, which was the same as used in the extraction equipments, was added. The mixture was vigorously shaken for 3-5 minutes and separated after 2-3 hours when the two phases were completely settled at room temperature ($20 \pm 2^{\circ}\text{C}$).

The concentration of acetic acid in the aqueous phase was determined by titration with standard sodium hydroxide. The organic phase failed to give up its acid promptly with ordinary stirring, making the titration slow and uncertain. A magnetic stirrer was employed and this accelerated the rate at which the acid passed from the organic phase into water. Even under these conditions, the end point was not as accurate as it was in the water. The acid seemed to have a slight tendency to remain in the organic phase.

A back titration method was used for the analysis of the organic phase. An excess of standard NaOH was added to the organic sample with phenolphthalein under intense agitation by magnetic stirrer and then standard HCl was used for the back titration. Careful titration was needed due to the low concentration of acetic acid in the organic phase. The material balance of acetic acid has been checked and the data which gave acid loss less than 5% were taken and plotted in Fig. 15. The distribution coefficient (m) appears to be approximately 0.0045. An experimental result for the solubility and partition ratio of acetic acid

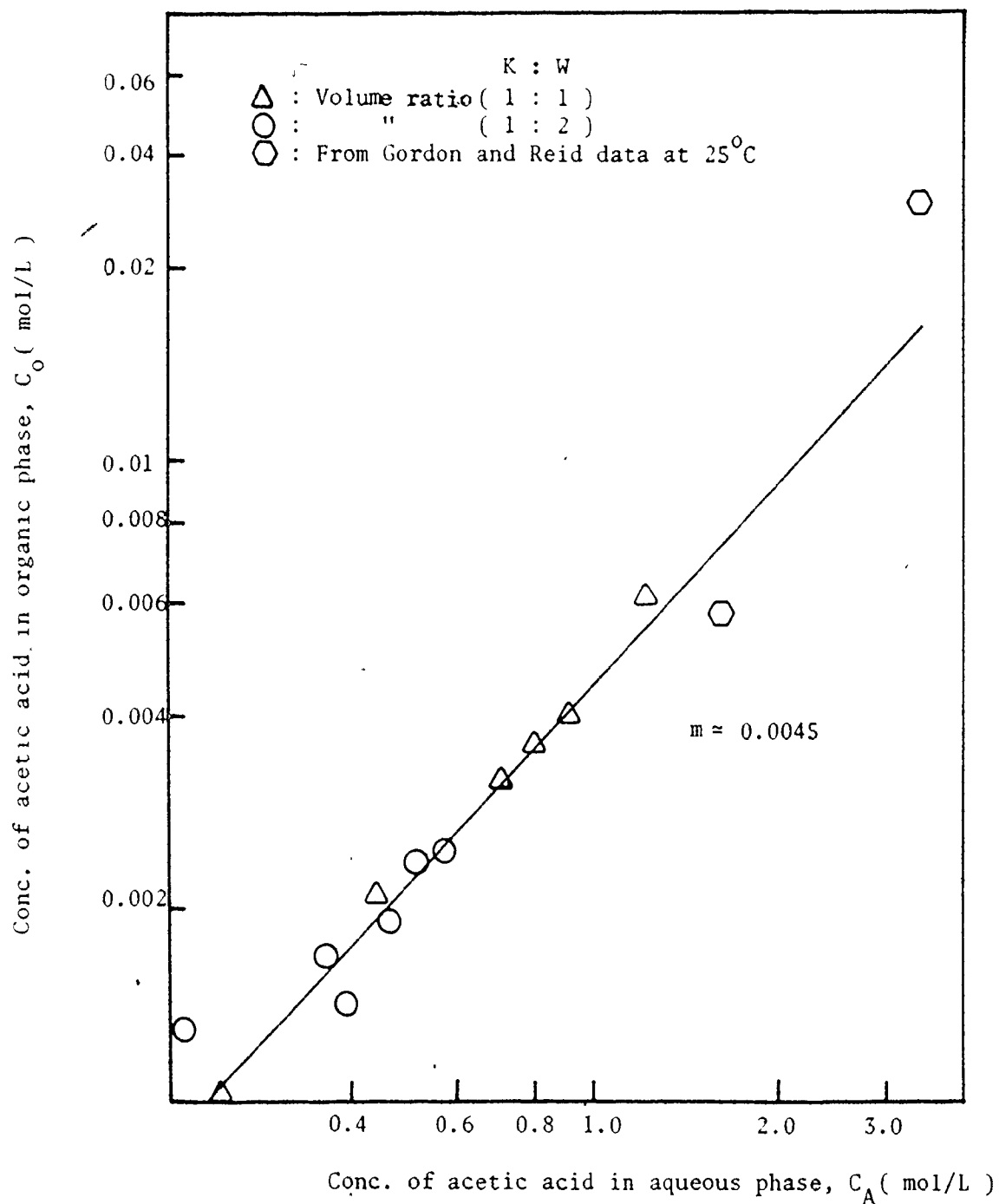


Figure 15. Equilibrium line in Kerosene-Acetic acid-Water system at room temperature ($20 \pm 2^\circ\text{C}$)

between kerosene and water was reported in the organic phase concentration range of 6×10^{-3} mol/L and 0.26 mol/L by Gordon and Reid (24). Some of the data obtained by Gordon and Reid, who used kerosene which was distilled between 180°C and 260°C , are also plotted in Fig. 15.

In the cocurrent operation, only one equilibrium stage is available. The equilibrium relationship is expressed in terms of molar concentration of acetic acid in each phase and a schematic representation (not to scale) of an operating line is shown in Fig. 16, assuming that the solutions are very dilute. A point on the operating line represents the bulk-averaged concentrations in each phase of the stream of any section of the column and the slope is determined by the flow ratio of two phases. Consequently, the line passes from the point representing the phases entering the column to that representing the effluent stream. The driving force for mass transfer is proportional to the distance between a point on the operating line and the extended point on the equilibrium line, as shown in Fig. 16.

4.2 Sampling and Analysis of Exit Streams

Let us consider the mass transfer operation conducted in a steady-state cocurrent fashion, as shown in Fig. 17. Denote C_A and C_O as the concentrations of acetic acid in the

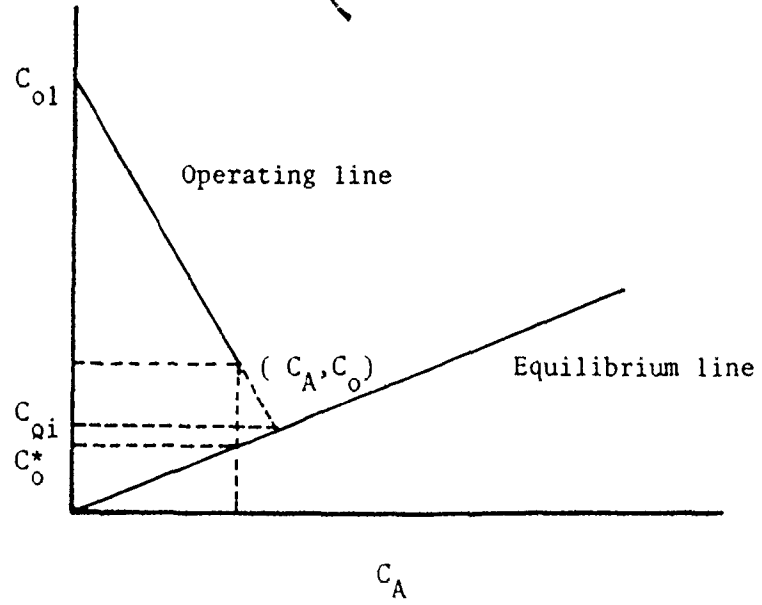


Figure 16, Operating and Equilibrium lines

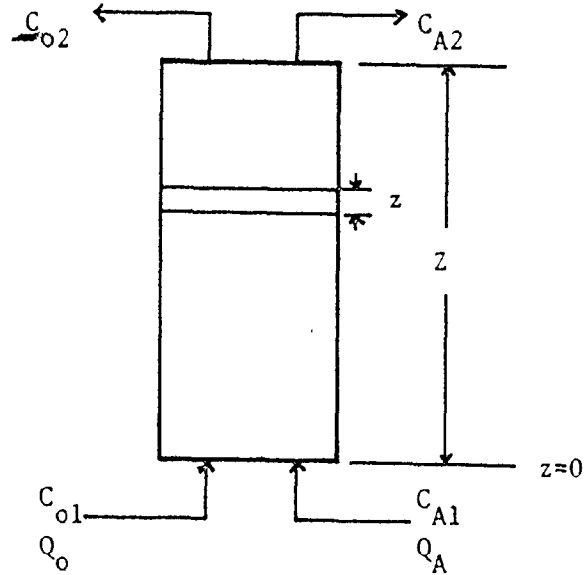


Figure 17. Material balance in a cocurrent extraction column.

aqueous phase and the organic phase, respectively. The water is assumed not to diffuse into the dispersed kerosene, which was presaturated with water. The material balance of acetic acid on the control volume gives

$$d\dot{m} = aS dz(C_o - C_o^*)K_o \quad 4-1$$

$$= Q_A d C_A \quad 4-2$$

$$= - Q_o d C_o \quad 4-3$$

Assuming that the flow in the column is plug flow, we get from the material balance between z and 0 .

$$C_A = \frac{Q_o}{Q_A} [C_{o1} - C_o] \quad 4-4$$

From the equilibrium relation, $C_o^* = mC_A$, we have

$$C_o^* = \frac{mQ_o}{Q_A} (C_{o1} - C_o) \quad 4-5$$

Rearrangement of equations 4-1 and 4-3 after substitution of C_o^* gives

$$dz = \frac{Q_o}{K_o a S} \frac{dC_o}{A C_{o1} - (1 + A) C_o} \quad 4-6$$

where $A = m Q_o / Q_A$. This is the Extraction Factor as used in standard mass transfer texts such as Treybal (25). Integration with boundary condition assuming that $K_o a$ is constant provides

$$\text{At } z = 0, \quad C_o = C_{o1}$$

$$\frac{1}{K_o a} = \frac{-Q_o}{S z} \cdot \frac{1}{1 + A} \ln \left[(1 + A) \frac{C_o}{C_{o1}} - A \right] \quad 4-7$$

In the present case of a very small m but Q_o in the same order as Q_A , the extraction factor is negligible, so this can reduce to

$$\overline{K_o a} = \frac{-Q_o}{Sz} \ln \frac{C_o}{C_{o1}}$$

or

$$\overline{K_o a} = \frac{-u_o}{z} \ln \frac{C_o}{C_{o1}}$$

4-8

In the preliminary experiments, samples were taken in a 250 mL separatory funnel after a steady condition was achieved, and then the aqueous phase and the organic phase were taken for analysis as soon as a clear layer was observed at the top and the bottom of the funnel. Phase separation in most of the runs has been achieved within 30 seconds due to the high interfacial tension of kerosene and water (34 mN/m).

The mass transfer product ($\overline{K_o a}$) was estimated from the concentration of acid in the organic phase of the effluent streams. The results have been compared with those of the indicator colour change method in Section 6.5.

4.3 Indicator Colour Change Method

As noted in Section 1.3, instantaneous chemical reaction in the presence of an indicator has been a useful means of measuring effective concentration profiles and

hence in the determination of axial dispersion coefficients. In this work, the technique is extended to the determination of mass transfer rates.

In the cocurrent extraction of acetic acid by dilute aqueous caustic solution, the acetic acid is transferred from kerosene droplets and then reacts instantaneously with dilute sodium hydroxide. The height in the column at which all the sodium hydroxide is reacted may be visually observed as a "neutralization zone" in the presence of an indicator (phenolphthalein); the zone appears as a sharp colour boundary within the plate stack of the column (17).

Let us consider a steady state mass balance of acetic acid in a control volume of the column with the assumptions that the mass transfer resistance lies mainly on the organic (dispersed) phase due to the small distribution coefficient and the reaction-enhanced aqueous phase mass transfer coefficient, as discussed in Section 4.1. Because the superficial velocities of the streams in the order of 20 cm/s are possible, the large Peclet number leads one to assume that the streams pass through the column in plug flow. Thus a material balance equation of acid in the dispersed (organic) phase can reduce to

$$u_o \frac{dC_o}{dz} + K_o a C_o = 0 \quad 4-9$$

With the assumed boundary condition at the bottom of the plate stack,

$$C_o = C_{o1} \quad \text{at } z = 0$$

we get

$$C_o = C_{o1} \exp\left(-\frac{1}{u_o} \int_0^z K_o a \, dz\right) \quad 4-10$$

In the aqueous phase, free sodium hydroxide is present below the neutralization zone ($z < z_n$), while free acid is present for $z > z_n$. Because the acetic acid being transferred from the organic phase reacts on a mole for mole basis with the free caustic solution at the neutralization zone, the acid transferred for $z < z_n$ must balance the caustic fed, i.e.

$$u_o (C_{o1} - C_o) = u_A C_{A1} \quad \text{at } z = z_n$$

Hence at $z = z_n$

$$\frac{C_o}{C_{o1}} = 1 - \phi \quad 4-11$$

where

$$\phi = \frac{u_A C_{A1}}{u_o C_{o1}}$$

The parameter ϕ is the molar ratio caustic fed in the aqueous phase to acid fed in the organic phase. Substituting equation 4-11 in equation 4-10 for $z = z_n$ provides

$$\frac{1}{u_0} \int_0^{z_n} K_0 a \, dz = -\ln(1 - \phi) \quad 4-12$$

Differentiation at $z = z_n$ and rearrangement gives

$$(K_0 a)_{z_n} = u_0 \frac{d}{dz_n} (-\ln(1 - \phi)) \quad 4-13$$

The analysis of the reciprocal slope of z_n vs. $-\ln(1 - \phi)$ plot permits the calculation of local mass transfer rate.

The averaged mass transfer product $(K_0 a)$ is calculated by assuming $K_0 a$ is constant throughout the region $0 < z < z_n$, whereby

$$\overline{K_0 a} = -\frac{u_0}{z_n} \ln(1 - \phi) \quad 4-14$$

The neutralization zone can be moved along the column by altering the concentrated caustic injection rate (and hence, effectively, ϕ) under the constant agitation and uniform flow conditions in order to estimate the local mass transfer rate.

The averaged mass transfer rate can be measured from the observation of the colour boundary and the use of Eq. 4-14 for various values of reciprocation frequency or flow conditions.

The experiment must obviously be performed with ϕ less than unity in order that the neutralization can occur within the column.

This method is considered to be much better than sampling and analysis of the effluent streams, which tend to undergo mass transfer during the sampling procedure and phase separation.

CHAPTER 5
MASS TRANSFER MODELS

5.1 N.T.U. and H.T.U. in Cocurrent Plug Flow

It is not strictly appropriate to apply the equilibrium stage concept in a differential mass transfer contactor such as spray tower, packed column, pulsed column, etc. because no discrete stages can be identified. In such differential types of contactor, equilibrium between phases is never reached and mass transfer rate is, therefore, very important in the design procedure. In such contactors, the transfer unit concept is useful as a counterpart of the equilibrium stage and is defined for cocurrent extraction as follows.

Integration of mass balance equation 4-6 between the bottom and the top of column gives a relationship for a column height in terms of the concentration change assuming that both the equilibrium and the operating lines are straight.

$$dz = \frac{Q_o}{K_o a S} \cdot \frac{dC_o}{AC_{o1} - (1+A) C_o} \quad 4-6$$

$$z = \left(\frac{Q_o}{K_o a S} \right) \int_{C_{o1}}^{C_{o2}} \frac{dC_o}{AC_{o1} - (1+A) C_o} \quad 5-1$$

The integral can be evaluated

$$\int_{C_{o1}}^{C_{o2}} \frac{dC_o}{AC_{o1} - (1+A)C_o} = \frac{-1}{1+A} \ln \left[(1+A) \frac{C_{o2}}{C_{o1}} - A \right] \quad 5-2$$

This integral is dimensionless and is defined as the number of transfer units (N.T.U.) based on the overall organic phase driving force. Obviously the N.T.U. and hence the contactor length (z) required, increases as the difference between C_{o1} and C_{o2} is increased.

In the kerosene-acetic acid-water system, the distribution coefficient (m) is small enough to be neglected, hence Eq. 5-2 can be simplified and the N.T.U. becomes merely

$$(N.T.U.)_o = \ln \frac{C_{o1}}{C_{o2}} \quad 5-3$$

The factor ($Q_o/K_o a S$ or $u_o/K_o a$) in equation 5-1 is known as the height of a transfer unit (H.T.U.). It is a characteristic of hydrodynamic conditions such as the flow rate and the specific interfacial area (a), but is taken to be independent of changes in concentration of the solute. It is important that the H.T.U. be specified correctly in regard to the phase and driving force considered; in this case it relates to the overall mass transfer driving force in the organic phase. The H.T.U. may vary with height because of changes in drop size, etc. An average value is

usually taken assuming no variation with height.

The overall mass transfer resistance $1/K_o$ consists of contributions from each phase, so that the overall H.T.U. is also the sum of two contributions;

$$(\text{H.T.U.})_o = \frac{u_o}{k_o a} + \frac{mu_o}{u_A} \left(\frac{u_A}{k_A a} \right) \quad 5-4$$

$$= (\text{H.T.U.})_o + A (\text{H.T.U.})_A \quad 5-5$$

Since A can be assumed to be negligible, we have

$$(\text{H.T.U.})_o = (\text{H.T.U.})_o$$

Thus the organic phase height of a transfer unit is the main contributor to the overall height of a transfer unit in this extraction process. In normal operating practice, however, the extraction factor (A) is chosen to be not greatly different from unity, usually within the range of 0.5-2.

5.2 Holdup

Holdup, defined as volume fraction of the dispersed phase in the column, is a function of agitation intensity, phase flow rate, and the physical properties such as density difference, viscosity, and surface tension.

In the countercurrent operation, the density difference which is the driving force causing the light phase to rise is considered to be important in determining the slip velocity. The holdup in the cocurrent extraction, however, can be estimated from the flow rates of the

continuous phase and the dispersed phase assuming no slip condition between two phases.

$$\epsilon = \frac{Q_o}{Q_o + Q_A} \quad 5-6$$

or

$$\epsilon = \frac{u_o}{u_o + u_A} \quad 5-7$$

This might slightly overestimate the actual holdup, because the density difference can increase the rising velocity of organic phase and result in lower holdup. However, at high flow rates (in the order 10 cm/s) and short contact times, the no slip assumption is approximately valid in this cocurrent extraction process. This assumption can be justified by the experiments of Seewald (26) who indicated that the holdup in cocurrently upward flow could be considered to be the flow ratio of the dispersed phase to the total phase at high energy dissipation per unit volume.

5.3 Specific Interfacial Area and Droplet Size

The hydrodynamic and mass transfer characteristics of Karr type of reciprocating plate column have been thoroughly investigated in the last two decades. The contact area of the dispersed phase and the continuous phase is one of main

design variables and is generally expressed in terms of a specific surface area (a), which is well known to be

$$a = \frac{6\varepsilon}{d_{32}} \quad 5-8$$

The holdup (ε) and Sauter mean diameter of droplet (d_{32}) are determined by the system's physical properties, the flow conditions, and the agitation intensity.

The Sauter mean diameter of dispersed droplets was correlated with the energy dissipation and system properties by Baird and Lane (8) who applied the Kolmogoroff isotropic turbulence concept (extended by Hinze) to the same column as used in this work. However, it was run countercurrently without mass transfer in several organic-aqueous systems. The following relationship was suggested by Baird and Lane for the fairly well agitated system.

$$d_{32} = 0.36 \frac{\gamma^{0.6}}{\bar{\rho}^{0.2} \psi^{0.4}} \quad 5-9$$

The coefficient 0.36 is empirical but dimensionless. This equation has been found to give fairly good agreement with the experimental results obtained by photographic measurement when Af is greater than 4 cm/s. At very high agitation, however, equation 5-9 tends to give smaller droplet diameters than those obtained from experiments. This might result in the prediction of larger interfacial surface area.

The holdup (ϵ) as discussed in the previous section, is given by Eq. 5-7.

$$\epsilon = \frac{u_o}{u_o + u_A} \quad 5-7$$

Substitution of ϵ and d_{32} in equation 5-8 gives

$$a = \frac{6}{0.36} \left(\frac{u_o}{u_o + u_A} \right) \left(\frac{\bar{\rho}^{0.2} \psi^{0.4}}{\gamma^{0.4}} \right) \quad 5-10$$

where

$$\bar{\rho} = \epsilon \rho_o + (1-\epsilon) \rho_A \quad 5-11$$

The energy dissipation per unit volume (ψ) might be considered to be composed of two terms; one is due to the pulsation of the plates, the other is due to the steady flow of fluid.

The power dissipation per unit volume due to pulsation was calculated using the quasi-steady friction concept proposed originally by Jealous and Johnson (27) for the pulsed columns, and the equation was corroborated for the reciprocating plate columns at normal stroke and frequency ($0.634 \text{ cm} < A < 2.54 \text{ cm}$, $0.5 \text{ Hz} < f < 6.3 \text{ Hz}$) by Baird and Hafez (10) as;

$$\psi_p = \left(\frac{2\pi^2}{3} \right) \cdot \bar{\rho} \left[\frac{1 - \sigma^2}{2 C_o \sigma^2} \right] (Af)^3/h \quad 5-12$$

The frictional energy dissipation due to steady flow has been estimated using the pressure drop along the column

calculated from the orifice equation. The pressure drop per plate in the orifice flow is given by

$$\Delta p = \frac{1}{2} \bar{\rho} (u_o + u_A)^2 \left[\frac{1 - \sigma^2}{C_o^2 \sigma^2} \right] \quad 5-13$$

Hence

$$\psi_s = \frac{1}{2} \bar{\rho} (u_o + u_A)^3 \left[\frac{1 - \sigma^2}{C_o^2 \sigma^2} \right] / h \quad 5-14$$

Therefore the total energy dissipation per unit volume becomes

$$\psi = \frac{\bar{\rho}}{h} \left(\frac{1 - \sigma^2}{C_o^2 \sigma^2} \right) \left[\frac{2\pi^2}{3} (Af)^3 + \frac{1}{2} (u_o + u_A)^3 \right] \quad 5-15$$

The ratio of the contribution of agitation to that of steady flow is given by

$$\frac{\psi_p}{\psi_s} = \frac{4\pi^2}{3} [Af / (u_o + u_A)]^3 \quad 5-16$$

Substitution of ψ in equation 5-10 yields

$$a = \frac{6}{0.36} \left(\frac{u_o}{u_o + u_A} \right) \cdot \frac{\bar{\rho}^{0.2}}{\gamma^{0.6}} \cdot \left\{ \frac{\bar{\rho}(1-\sigma^2)}{h C_o^2 \sigma^2} \left[\frac{2\pi^2}{3} (Af)^3 + \frac{1}{2} (u_o + u_A)^3 \right] \right\}^{0.4} \quad 5-17$$

The contribution of steady flow is generally negligible in countercurrent operation but is significant at

low agitation in the present cocurrent operation in which the superficial velocity of the steady flow is in the order of 10 cm/s.

Caution is necessary in applying this equation to situations where energy dissipation is very low. Under such conditions, the isotropic turbulence assumption may not be valid because the energy dissipation tends to be concentrated near each plate. Also the breakup of droplets by collision with the plates may be significant at low agitation.

5.4 Mass Transfer Coefficient (K_o)

For designing liquid-liquid extraction equipment, a good knowledge of the dispersed phase and the continuous phase mass transfer coefficients is required to estimate the overall mass transfer coefficients.

Many studies of mass transfer coefficients both inside and outside a single droplet have been published in the last three decades. The subject appears to be well understood for cases where the drop retains an approximate spherical shape and where the drop does not oscillate and interfacial turbulence is absent. The basic results obtained from the studies on behaviour of single droplet have been applied to the multiparticle system in which the particles are freely suspended. It was known that the

presence of another single neighbouring particle does not affect the mass transfer rate unless the distance between the particle surface is smaller than $1.5 d_p$ (28).

The overall mass transfer coefficient based on the organic (dispersed) phase can be predicted in general from

$$\frac{1}{K_o} = \frac{1}{k_o} + \frac{m}{k_A} \quad 5-18$$

where k_o and k_A are organic phase and aqueous phase film coefficients, respectively. In the kerosene-acetic acid-water system, the distribution coefficient, m , as discussed in the previous section, is small enough to justify the assumption that the mass transfer resistance would mainly lie in the organic (dispersed) phase and the overall mass transfer coefficient (K_o) might be approximately equal to the organic phase film coefficient (k_o).

Various theoretical models have been proposed for the estimation of dispersed phase mass transfer coefficients. These models may be broadly classified as (i) stagnant drop models, and (ii) internal circulation models (involving various assumptions of internal circulation patterns such as Hadamard streamlines, Stokes streamlines, and turbulent internal eddy motion) (25, 29, 30).

For rigid spheres with no circulation, Treybal (25) suggested the following relationship for the mass transfer coefficient (k_o) assuming that mass transfer takes place by

pure molecular diffusion and the continuous phase resistance is completely absent.

$$k_o = \frac{2\pi^2}{3} \frac{D_{AB}}{d_p} \quad 5-19$$

For circulating drops, the analysis of Kronig and Brink (29) using Hadamard stream lines gives the following relationship:

$$\bar{k}_o = 17.9 \frac{D_{AB}}{d_p} \quad 5-20$$

It should be noted that equation 5-20 is similar to equation 5-19 except for the pre-coefficient which is about 2.56 times greater.

Various correlations for mass transfer coefficients, both the continuous phase and the dispersed phase, have been extensively summarized by Laddha and Degaleesan (31).

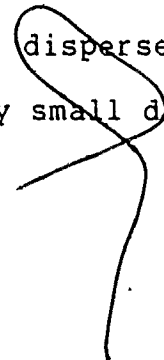
A relatively high intensity of agitation generated in Karr column creates very small droplets (typically less than 0.1 cm diameter) which might be considered to be rigid spheres due to the stabilizing effects of interfacial tension. The Treybal model has been applied to the well agitated system. At low agitation, the droplets formed might be big enough to permit internal circulation and the Kronig and Brink model could be employed to predict the dispersed phase mass transfer coefficient.

5.5 Prediction of $\overline{K}_O a$ and Column Height

A good estimation of the overall mass transfer coefficient and specific surface area is considered to be a major design requirement for mass transfer equipment. The mass transfer performance is characterized by the H.T.U. and the N.T.U. as discussed in the previous section. The former parameter, height of a transfer unit, characterizes the physical properties of the system such as configuration of apparatus and hydrodynamic conditions. The latter, the number of transfer units, represents the composition change per unit driving force in a given piece of equipment. As can be seen from Eq. 5-1, the mass transfer product $\overline{K}_O a$ is a major term in the estimation of H.T.U.

In this work, $\overline{K}_O a$ has been calculated by combining overall mass transfer coefficient and the specific surface area as predicted in Sections 5.3 and 5.4.

Equation 5-17 was used to estimate a specific surface area with the assumption that the mass transfer might not affect the interfacial tension of the system, because a low concentration of organic phase has been employed and acetic acid is not highly surface active. The Treybal model has been used for the dispersed phase mass transfer coefficient in case where very small droplets could be generated by high agitation.



From equations 5-17 and 5-19, $K_o a$ is given by

$$\overline{K_o a} = \left(\frac{2\pi^2}{3}\right) \left(\frac{6}{0.36}\right) \left(\frac{D_{AB}}{d_{32}}\right) \left(\frac{u_o}{u_o + u_A}\right) \left(\frac{\rho}{\gamma}\right)^{0.6} \left(\frac{1 - \sigma^2}{C_o \sigma^2 h}\right)^{0.4}$$

$$\left\{ \frac{2\pi^2}{3} (Af)^3 + \frac{(u_o + u_A)^3}{2} \right\}^{0.4} \quad 5-21$$

A small computer program has been employed for the calculation of $\overline{K_o a}$.

At low agitation level, the circulating drop model was used instead of the Treybal model.

The height of plate stack required for a given performance can be estimated in terms of column efficiency. From the equations 5-3 and 5-4, the height of plate stack is given by

$$z = \frac{-u_o}{\overline{K_o a}} \ln \frac{C_{o1}}{C_{o2}} \quad 5-22$$

Column efficiency is defined as:

$$\eta = \frac{C_{o1} - C_{o2}}{C_{o1}} \quad 5-23$$

Thus, the height of plate stack for a given efficiency is given by substitution of η in equation 5-22.

$$z = \frac{-u_o}{\overline{K_o a}} \ln (1 - \eta) \quad 5-24$$

CHAPTER 6

MASS TRANSFER RESULTS AND DISCUSSION

6.1 Effect of ϕ on z_n ; Local Mass Transfer Product ($K_o a$)

Under constant agitation, the concentrated caustic flow rate has been varied within the limit that neutralization of the caustic could take place in the plate stack. The molar ratio of the caustic fed in the aqueous phase to the acid fed in the organic phase, ϕ , therefore must be equal to or less than one. The neutralization zone (z_n) has been changed between 20 cm and 140 cm from the base of the plate stack in order to minimize the entry and the end effects in the majority of experiments.

The plot of z_n vs. $-\ln(1-\phi)$ shown in Fig. 18 tends to give straight lines for the cases where the column was run without agitation or at low flow rate under high pulsation. The equilibrium droplet size distribution due to only the steady flow, as in the perforated column, might be rapidly achieved at the lower part of plate stack in case of no agitation. The high agitation and low flow rate would also produce uniform drop size along the column providing constant mass transfer product ($K_o a$). The plots, however, turned out curved in cases where the short residence time of

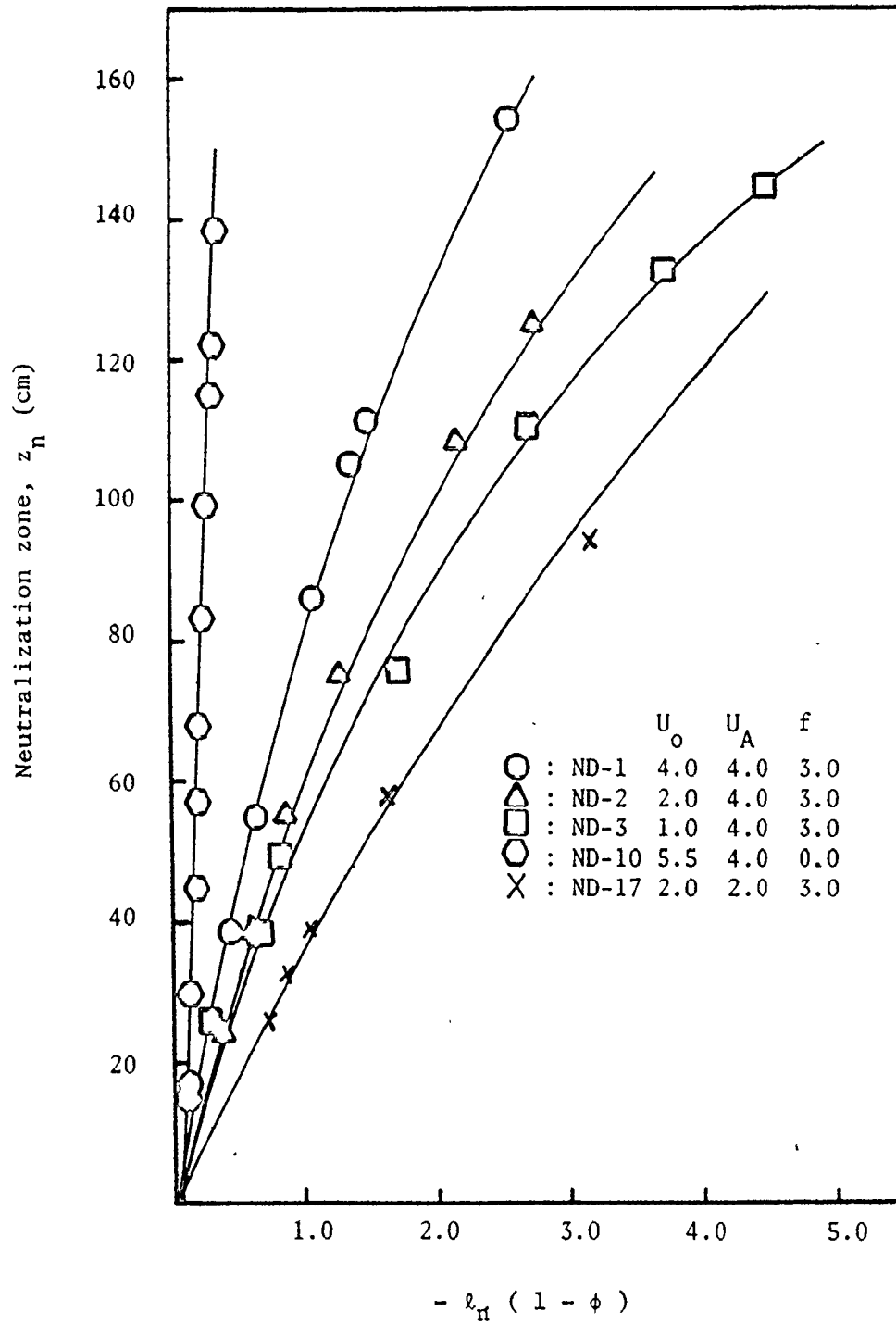


Figure 18. Neutralization zone (z_n) vs. $-l_n(1-\phi)$

the fluid due to the high flow rate might result in the incomplete breakup of drops even at the top of the plate stack.

A cubic-spline subroutine has been employed to analyse the slope of the curve which permits the calculation of the local mass transfer rate along the column.

There have been a few attempts to estimate the local mass transfer rate by employing the axial distribution of Sauter mean droplet diameters which has to be measured in the different types of equipment (32), but as far as it is known this is the first time the local $K_o a$ has been obtained by direct means.

A typical plot of local mass transfer product ($K_o a$) is given in Fig. 19. The local mass transfer product at high agitation and high flow rate appears to increase along the column because of the initially incomplete breakup of droplets. However, the local mass transfer product appears to be much higher near the bottom of the plate stack and decreases to be uniform above approximately 40 cm of plate stack, in the case of run ND-10 which was performed with a high flow rate at no agitation. This might be because the organic phase at the lower part of plate stack begins to be broken up to smaller drops by hitting the plate, resulting in a high initial value of K_o due to surface renewal. Another approach is to consider an "entry effect" beneath

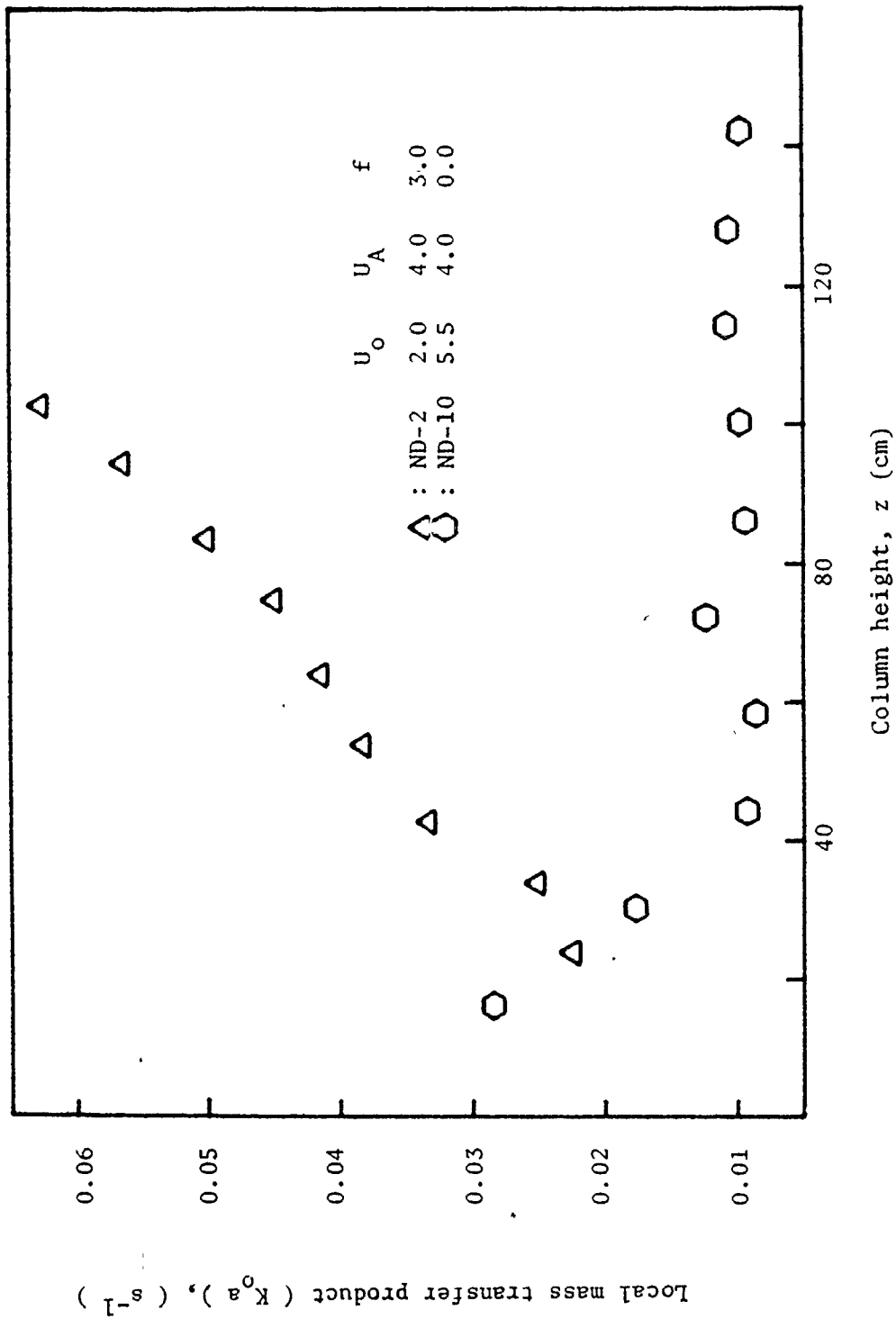


Figure 19. Local mass transfer product ($K_0 a$) vs. z

the plate stack: this could be analyzed by considering a particular $(K_o a z)_E$ acting before the dispersion reaches the plate stack, thus

$$\text{at } z = 0 \quad C_o = C_{o1} \exp \left[\frac{-(K_o a z)_E}{u_o} \right] \quad 6-1$$

$$\text{at } z > 0 \quad C_o = C_{o1} \exp \left[\frac{-\{(K_o a z)_E + (\overline{K_o a} z_n)\}}{u_o} \right] \quad 6-2$$

Therefore

$$1 - \phi = \exp \left[\frac{-\{(K_o a z)_E + (\overline{K_o a} z_n)\}}{u_o} \right] \quad 6-3$$

Hence

$$-\ln(1 - \phi) = \frac{(K_o a z)_E}{u_o} + \frac{\overline{K_o a} z_n}{u_o} \quad 6-4$$

Data of ND-10 were reported in Fig. 20. From the extrapolation of data points, we have $(K_o a z)_E \approx 0.07 u_o = 0.39 \text{ cm s}^{-1}$. The uniform $K_o a$ of the upper part of plate stack is approximately 0.01. Therefore the entry effect cannot be neglected in the cases of no agitation or low agitation.

6.2 Effect of Agitation

The mass transfer rate was significantly affected by the intensity of agitation which is mainly responsible for

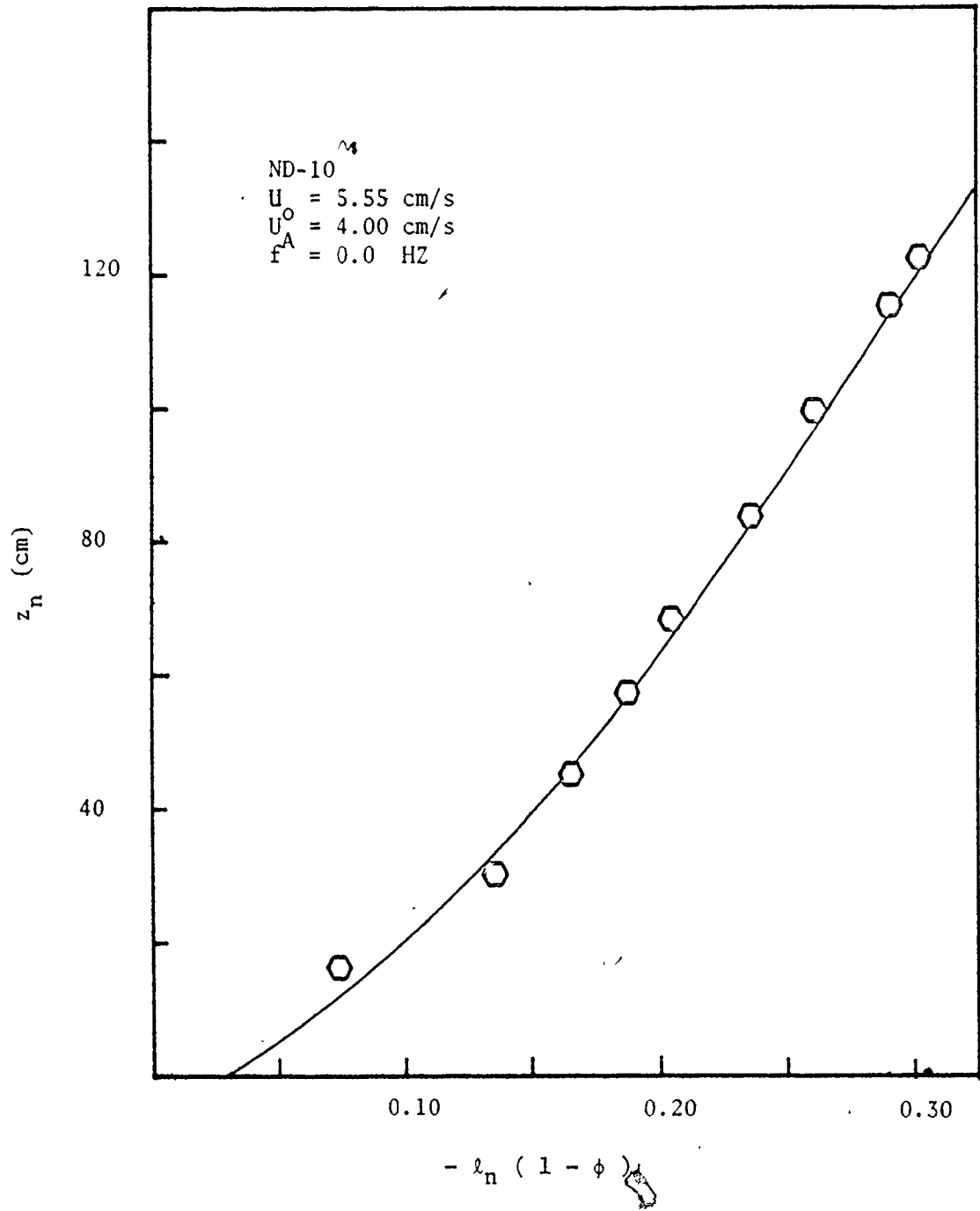


Figure 20. The analysis of entry effect for ND-10.

the breakup of droplets as discussed in Section 5.3. Some of the present experiments have been carried out under uniform flow conditions such that the variation of frequency causes the neutralization zone to move along the column. The neutralization boundary has travelled downwards as the frequency increases due to more specific surface area being created. No attempt to vary the amplitude has been made.

The plot of $\overline{K_0 a}/\epsilon$ vs. ψ is shown in Fig. 21, and the measured slope appears to be approximately 0.6, while the slope is expected to be 0.8 from the model (Eqs. 5-21 and 5-9).

A wide variation of frequency has been made in two sets of experiments (ND-15, ND-16). The data shown in Fig. 22 indicates that the prediction based on "Af" alone is exceeded when $Af < 7$ cm/s because of the additional contribution of steady flow friction to the total energy dissipation. It is noted that the slope of $\overline{K_0 a}/\epsilon$ vs. Af can be predicted from the following relationships assuming the stagnant drops.

$$\overline{K_0 a}/\epsilon = \frac{6 K_0}{d_{32}} \propto d_{32}^{-2} \propto \psi^{0.8} \propto (Af)^{2.4} \quad 6-5$$

The transition from the circulating drops to the stagnant drops at increasing Af will decrease the exponent below 2.4; the linear parts of the data plot in Fig. 22 show a slope of about 1.6.

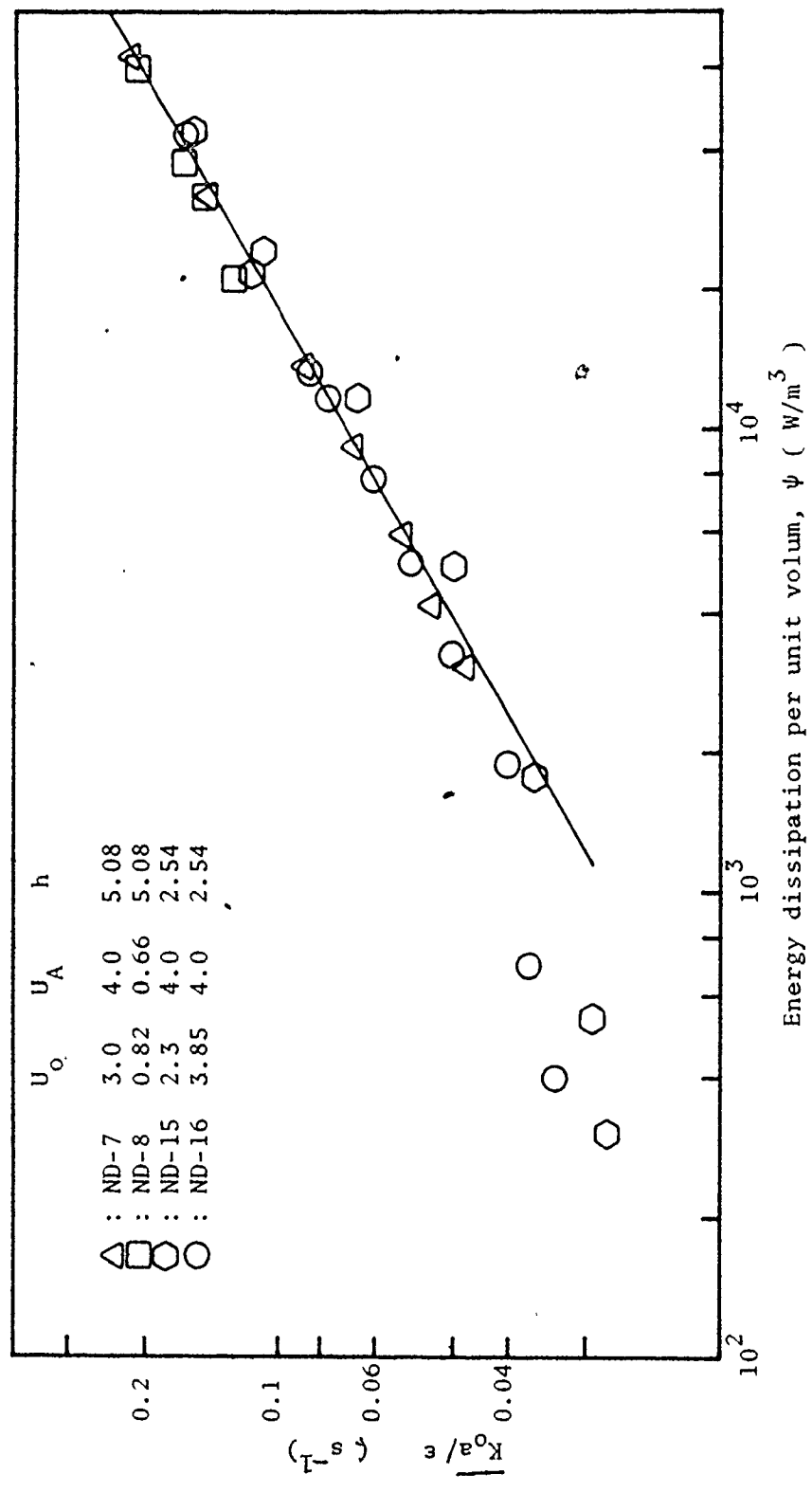


Figure 21. Effect of energy dissipation on K_{0a}/ϵ

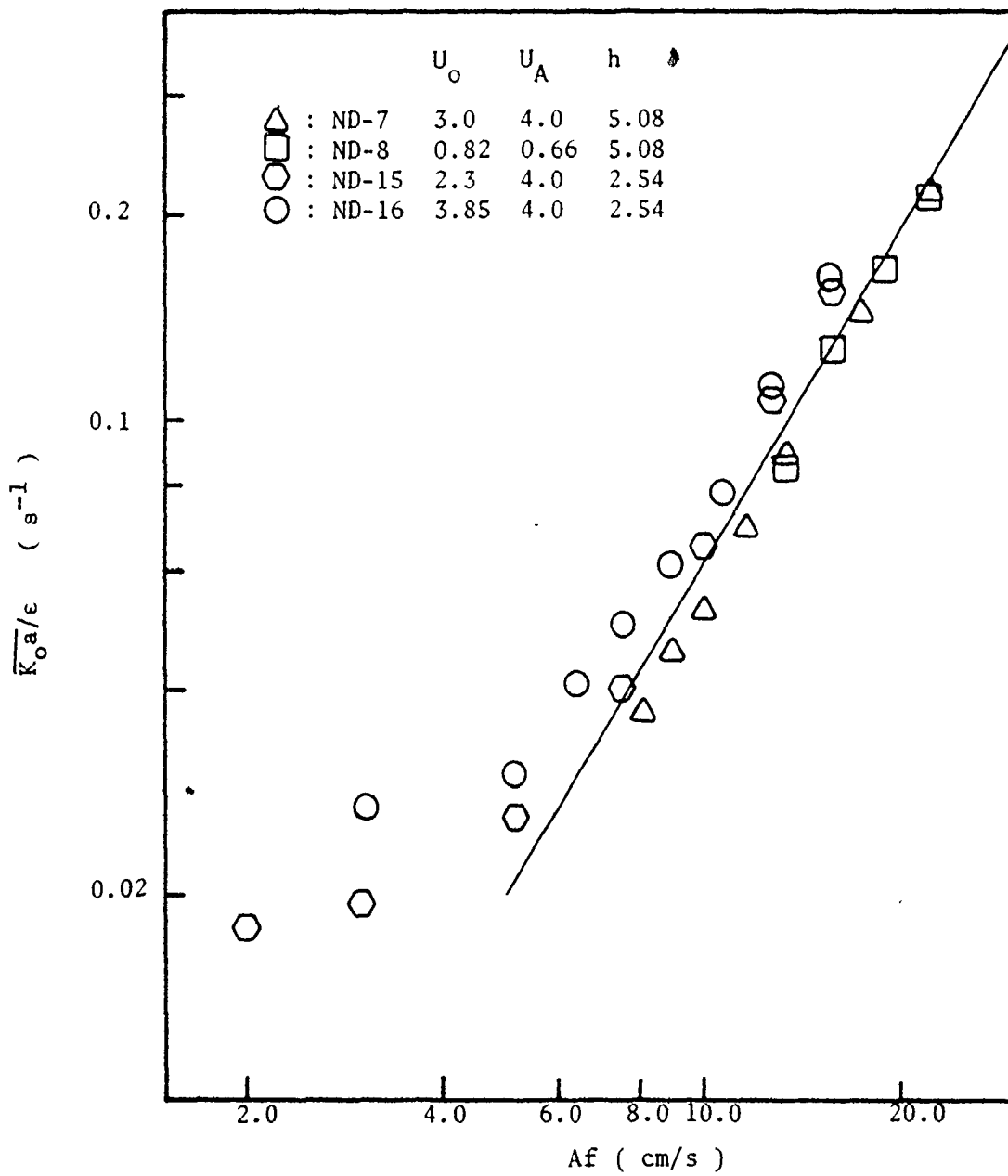


Figure 22. Effect of agitation on $\overline{K_o a} / \epsilon$

The spacing of 2.54 cm gives a slightly higher mass transfer rate, but the slope appears to be same as in the spacing of 5.08 cm at high A_f as shown in Fig. 20. This is to be expected because the specific energy dissipation ψ is greater at reduced plate spacing (Eq. 5-15).


The contribution of steady flow friction to the total energy dissipation should be included in the calculation of the specific surface area, especially at low agitation in this cocurrent operation; its effect might be negligible in the countercurrent operation at relatively low flow rates.

6.3 Effect of Flow

Differential countercurrent extractors are frequently subject to axial dispersion that severely reduces extraction rate because of the reduction of the concentration difference between two phases which is the driving force for the mass transfer. Substantially smaller concentration differences than those expected in plug flow are actually experienced in the countercurrent operation, depending on the Peclet number of the system.

In the cocurrent flow, there is no limitation of velocity by flooding and therefore very high velocities and agitation can be employed.

The majority of experiments was carried out with superficial velocity in the order of 10 cm/s resulting in



Peclet numbers greater than 100, which support the plug flow assumption made in the process of the derivation of mass balance equations.

The organic phase flow rate has been varied to move the neutralization zone along the column while the continuous phase flow rate, the caustic concentration, and the agitation were kept uniform.

The mass transfer rate tends to be linearly enhanced with the increase of organic flow at high agitation as shown in Fig. 23. It is also observed that under no agitation or low agitation, the mass transfer appears to improve quickly as the organic flow is increased. This might suggest that the kinetic energy of the steady flow plays a significant part in the rupture of droplet as the external agitation decreases. The contribution of the steady flow to the total energy dissipation can be estimated by equation 5-16. Intense agitation results in a negligible effect of the steady flow on creating drops. The improvement of mass transfer by agitation therefore mainly depends on the increase of holdup.

The averaged mass transfer product ($\overline{K}_o a$) divided by holdup (ϵ) has been plotted against the organic flow in Fig. 24. In case of ND-5, high organic flow might cause the incomplete breakup of droplets due to the short contact time, but then at very high u_o , the increased energy input by the

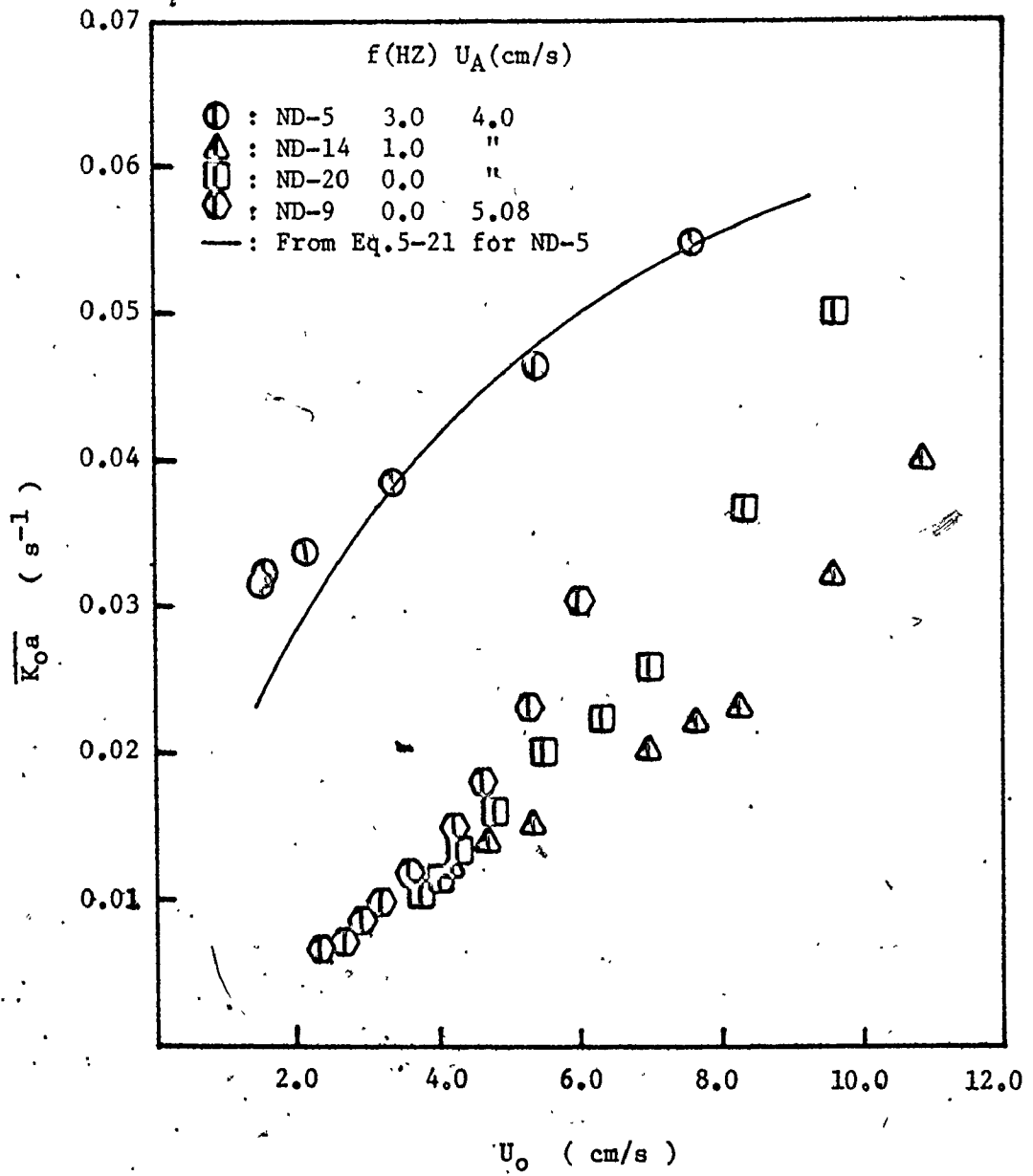


Figure 23. Effect of U_0 on mass transfer product ($\overline{K_0 a}$)

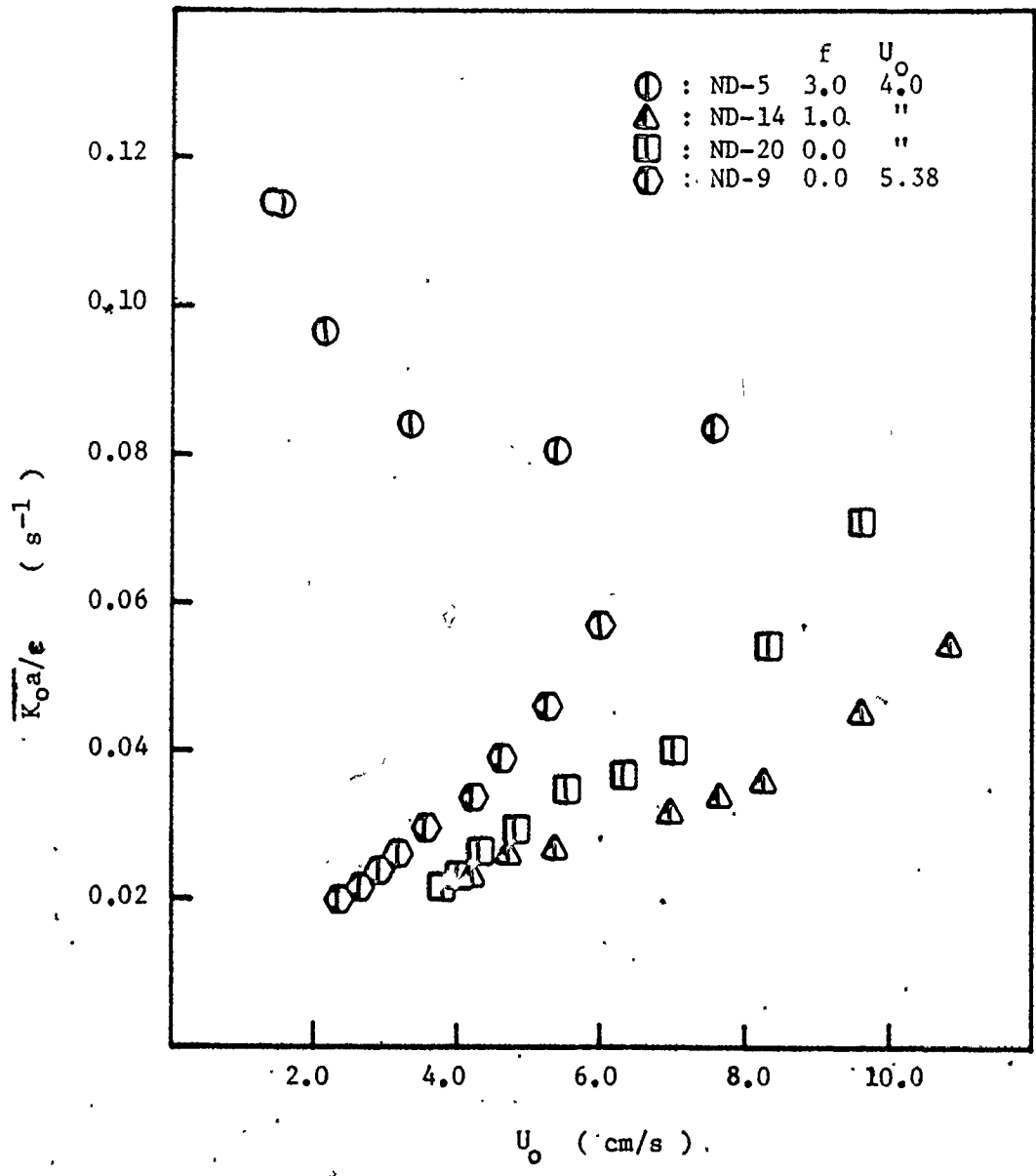


Figure 24. Effect of u_0 on K_0a/ϵ

steady flow can cause $\overline{K_0 a}/\epsilon$ to increase again. Therefore a minimum $\overline{K_0 a}/\epsilon$ is observed at about $u_0 = 5$ cm/s. At low agitation (ND-14 and ND-20), the effect of increasing u_0 on decreasing the drop size is clearly visible.

One set of runs (ND-6) (not shown in Fig. 24, see Table 4, Appendix C) was carried out with the variation of water flow rate while the organic flow, the concentrated caustic flow, and the agitation were not changed. No significant change in mass transfer rate has been indicated.

A quantitative comparison of total energy dissipation per unit volume with the minimum energy required to overcome the interfacial tension supports the effect of coalescence at low agitation (see Appendix B).

It is noted that some scatterings that data points of ND-14 were slightly less than those of ND-20 have been observed.

6.4 Effect of Plate Spacing

Various plate and baffle arrangements for the Karr type extraction column have been employed to study column performance and particularly the axial dispersion due to the circulation of fluid between plates which substantially reduces the column performance (3,7).

Two values of the plate spacing (h) have been used in this work, namely 2.54 cm and 5.08 cm. A slight improvement

of mass transfer can be observed in Figures 22 and 25 in case of smaller spacing. However, the increase of mass transfer seems not to be significant as Karr investigated the effect of various plate spacing on the column performance in countercurrent operation (3).

A sharper neutralization boundary has been observed with the smaller spacing, especially at low agitation at which the isotropic turbulence concept might be more likely applied to the smaller spacing than to the larger spacing.

6.5 Effect of Phase Inversion and Holdup

The phase inversion of a liquid-liquid dispersion is determined by the collision frequency and the coalescence frequency of the agitated dispersion. The phase inversion in kerosene-water system has been investigated by Ali (33). Rashmid and Jeffreys developed a model which predicts the phase inversion of the agitated dispersion and compared Ali's data with it (34).

The data of Ali (1969) for the kerosene-water system are given in Fig. 26 in which two curves separate three zones: zone (i) in which the composition of the mixture and agitation intensity are such that only water can exist as the dispersed phase, zone (ii) where either phase can be dispersed depending on the method by which the dispersion was formed, and zone (iii) in which only the kerosene can

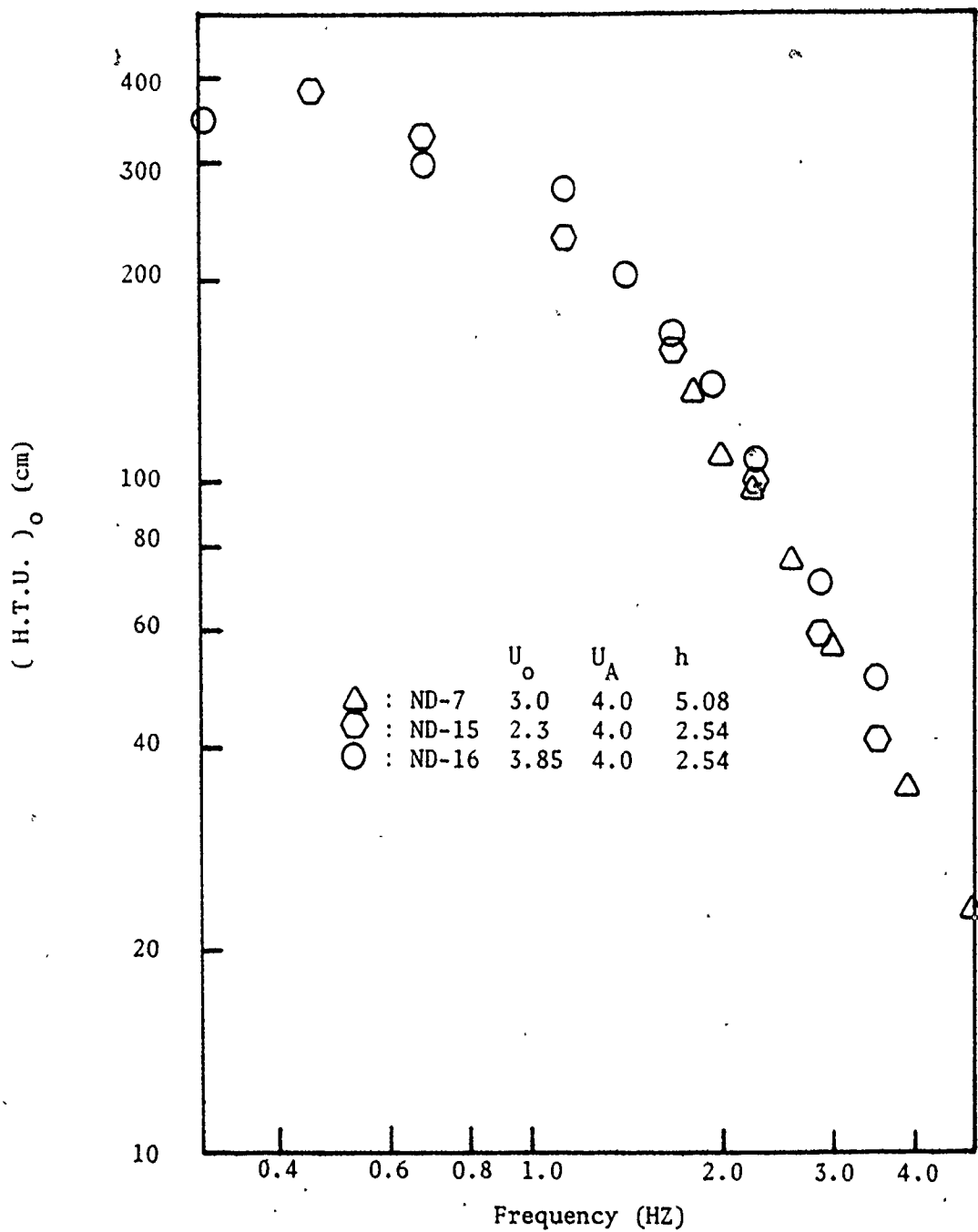


Figure 25. Effect of plate spacing on $(H.T.U.)_o$

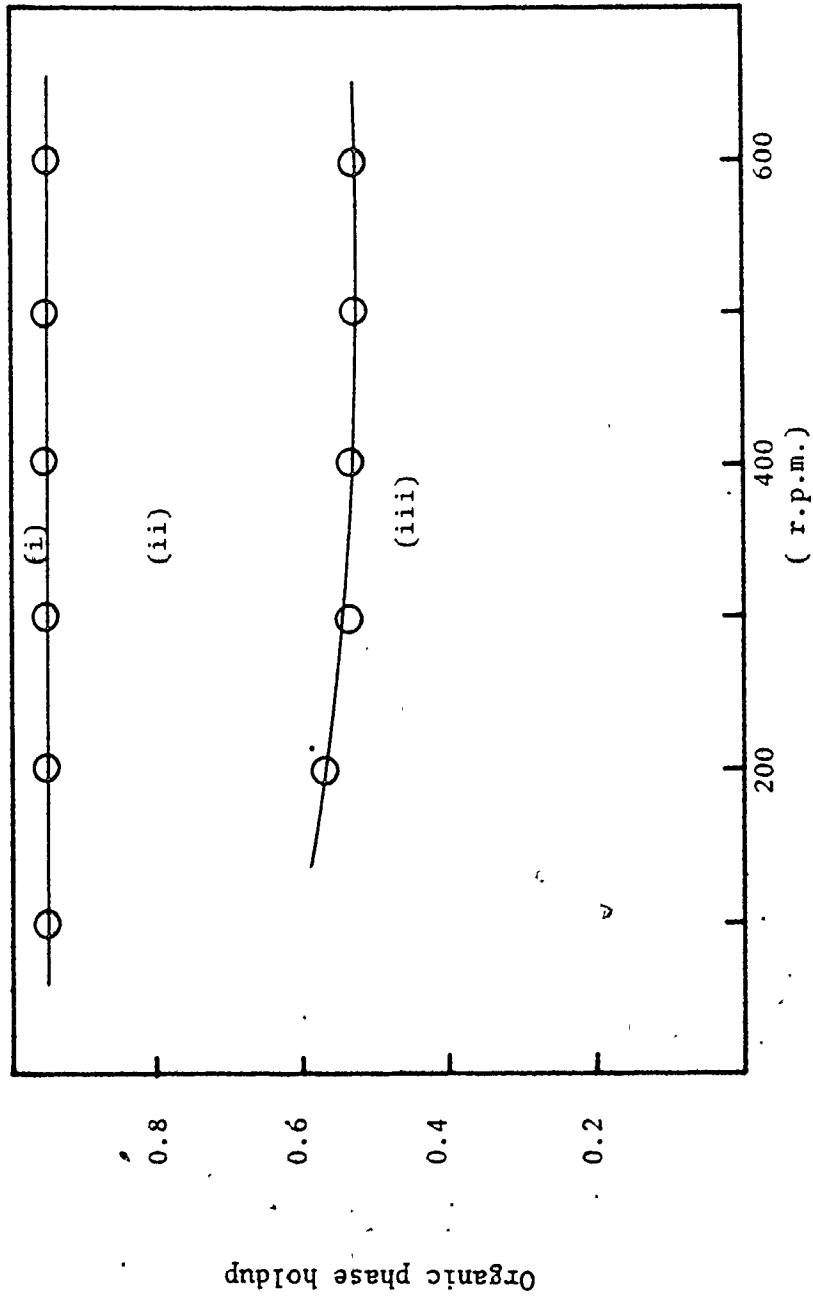


Figure 26. Phase inversion of Kerosene-Water system (replotted from Ali (1969))

exist as the dispersed phase.

In this cocurrent extraction, it was assumed that the organic phase was completely dispersed and no phase inversion took place in order to obtain a sharp neutralization zone. Most of the present experiments have been carried out such that the water was initially running and then kerosene was dispersed up to holdup 75%. The neutralization zone has been clearly seen at high agitation, which might imply that the kerosene was completely dispersed even in the ambivalence range as shown in Fig. 26. The coalescence of kerosene, however, has been observed at low agitation when the organic holdup exceeded 60%. Under these conditions, the neutralization boundary was somewhat diffused.

Some of the present runs have been done with the organic flow rate increasing at a constant aqueous flow rate, whereby the organic holdup and the total flow rate were increased.

The holdup effect on the mass transfer product ($\overline{K}_O a$) was shown in Fig. 27. At low agitation, holdup has a big effect, partly because of its direct contribution to $\overline{K}_O a$ and partly because of the importance of u_o in drop breakup. At high agitation, the drop size would be expected to be uniform but, since $a \propto \epsilon$, there should be a linear relationship, i.e. a slope of unity on the log-log plot. The shallower slope actually obtained could be due to an effect of

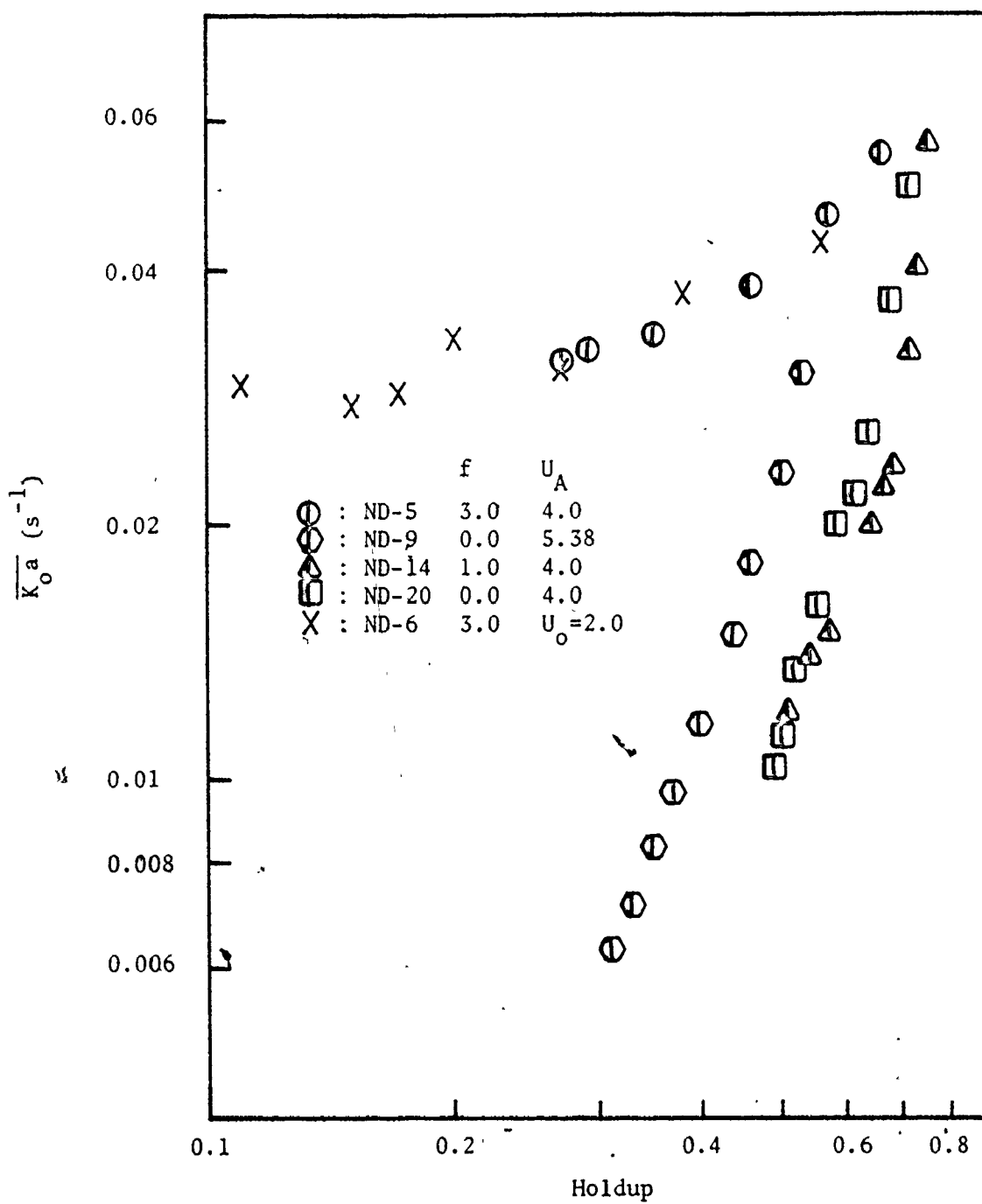


Figure 27. Effect of holdup on $\overline{K_o a}$

coalescence at high holdup, causing a reduction in \underline{a} below the expected value.

6.6 Comparison of $\overline{K_o a}$ Observed (this work) with $\overline{K_o a}$

Calculated

The average mass transfer product ($\overline{K_o a}$) predicted in Section 5.5 has been compared with the $\overline{K_o a}$ obtained by both indicator colour change method and the analysis of exit streams. It was observed in Fig. 28 that reasonable agreement is obtained with Eq. 5-21 (Treybal model) at high agitation. At low agitation, the data points trend higher than Eq. 5-21 and agree better with the circulating drop model which is simply Eq. 5-21 multiplied by a factor of 2.56 on the right hand side (see Eqs. 5-19 and 5-20). The large deviation of data points from the predicted values implies the relative importance of a collision mechanism of drop breakup in the absence of external agitation. A transition from the circulating drop model to the rigid sphere model is also observed due to the variation of drop size as agitation is increased (run ND-16). The data points of ND-9 and ND-20 might also indicate that the entry effect should be considered at low agitation as discussed in Section 6.1. It must be noted that at very high agitation, the calculated drop size has been found smaller than the observed drop size as indicated in Section 5.3 and this

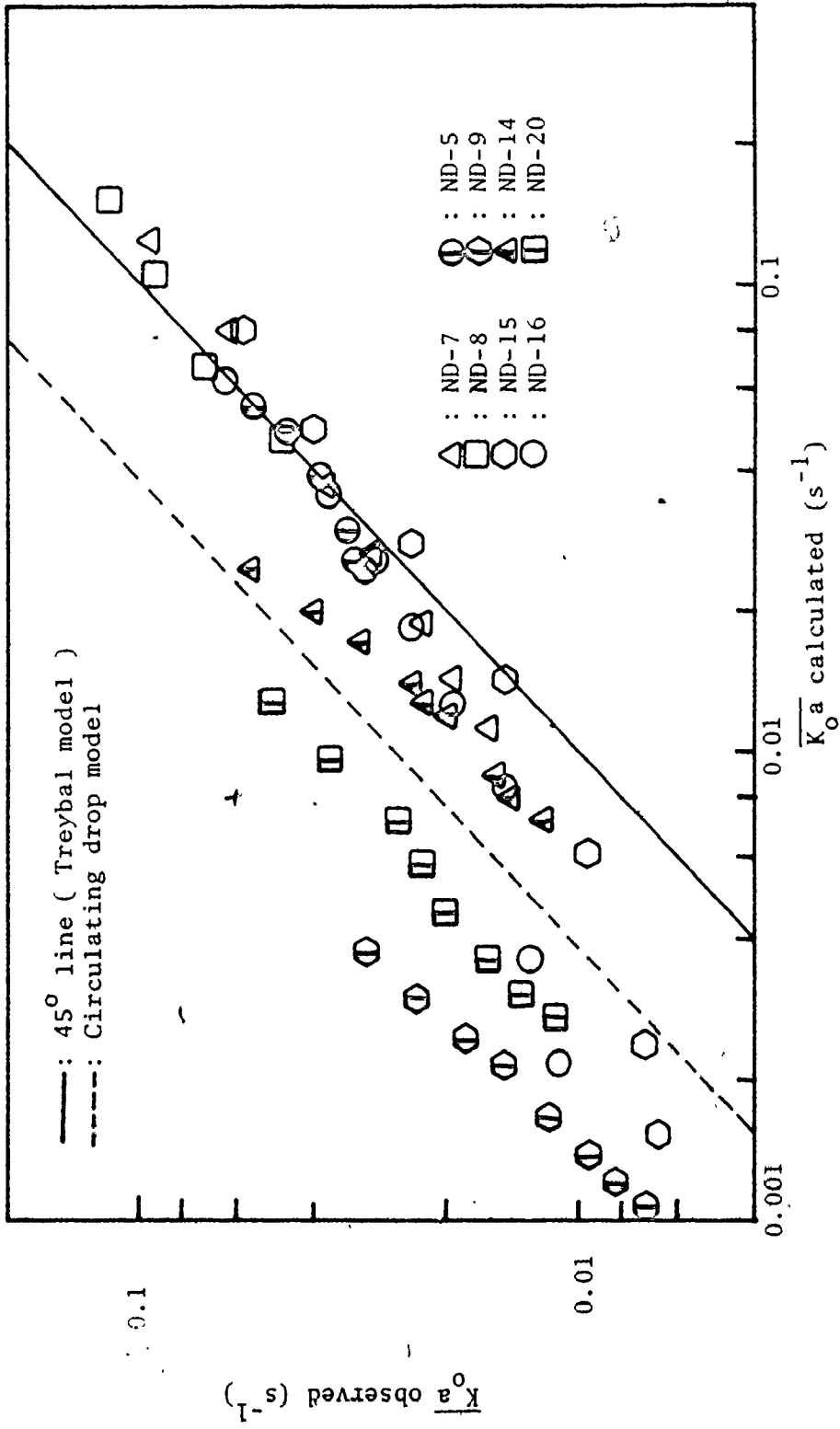


Figure 28. Comparison of $\overline{K_0a}$ observed (this work) with $\overline{K_0a}$ calculated.

might overestimate the $\overline{K_o a}$.

Some of the data obtained from the analysis of the exit stream are illustrated in Table 3 (Appendix C). The mass balance of acid in the data was checked and the mass transfer product ($\overline{K_o a}$) was calculated by the Eq. 4-8. The observed $\overline{K_o a}$ appears much larger than values obtained by the indicator colour change method under similar conditions. This result is probably due to the additional mass transfer during the sampling processes and in the section between the top plate and the exit nipple.

Some uncertainties in the model such as the applicable molecular diffusion coefficient, possible changes of interfacial tension and interface resistance due to contamination have contributed to the scatter of the points shown in Fig. 28. These factors cannot be accounted for accurately in one present state of knowledge. The data obtained by the indicator colour change method are tabulated in Table 4 (Appendix C).

6.7 Comparison of $\overline{K_o a}$ Observed (Karr (22)) and $\overline{K_o a}$ Calculated

Some cocurrent mass transfer data have been obtained by Karr (22) in a 2.54 cm Karr column in which o-xylene containing approximately 1% acetic acid was extracted concurrently by water. The volumetric flow ratio of o-xylene

to water was deliberately chosen to be 16 to 1 in all runs such that the extraction factor was unity and the water was dispersed in the xylene. Superficial velocities (total) ranged from 5.75 to 52.5 cm s⁻¹, i.e. considerably in excess of the values possible in this work.

The samples from the top of the column were taken conventionally in a separatory funnel after steady state operation of the column had been achieved. Then the respective samples were separated for analysis as soon as clear layers were observed at the top and bottom of the separatory funnel. The data obtained by Karr (22) have been summarized in Table 5 (Appendix C).

Because the distribution coefficient of acetic acid between water and o-xylene was approximately 1/16, it was assumed that the major mass transfer resistance in this case was in the organic (continuous) phase. A similar approach has been taken to compare the data with the predicted values. Most of the experiments have been run under very high agitation such that the droplets might be below 1.0 mm in diameter. Thus rigid sphere behaviour is likely and this suggests the employment of Levins' well-substantiated correlation (35) of the continuous phase Sherwood number as a function of agitation and system properties.

$$Sh_p = 2 + 0.47 \left[\frac{d_p^{4/3} \epsilon^{1/3}}{v} \left(\frac{D_s}{D_T} \right)^{0.28} \right]^{0.62} S_c^{0.36} \quad 6-6$$

where D_s/D_T , the ratio of impeller diameter to mixer diameter, is taken to be effectively 1 in this work.

The average mass transfer product ($\overline{K_o a}$) has been calculated using the Levins' correlation for the continuous phase mass transfer coefficient and the specific surface area calculated by Eq. 5-17. The average mass transfer product ($\overline{K_o a}$) was obtained from Karr's data (22) using Eq. 4-7. The stage efficiency (E) is defined as

$$E = \frac{C_{o1} - C_{o2}}{C_{o1} - C_{o2 \text{ eq}}} \quad 6-7$$

Substitution of Eq. 6-7 in Eq. 4-7 yields

$$\overline{K_o a} = - \frac{u_o}{(1 + A)Z} \ln (1 - E) \quad 6-8$$

where Z is the total height of plate stack.

A reasonable agreement of experimental data with the predicted values has been shown in Fig. 29. However the estimated $\overline{K_o a}$ seems to be slightly less than those observed in some cases. This could be due to the additional mass transfer due to the oscillation and the circulation of droplets while very small solid particles were suspended by stirring in Levins' work. It could also be considered that the mass transfer effects during sampling and separation might lead to overestimate the actual $\overline{K_o a}$. As discussed in the previous sections, $\overline{K_o a}$ measured by analysis of exit stream may be significantly higher than the actual $\overline{K_o a}$.

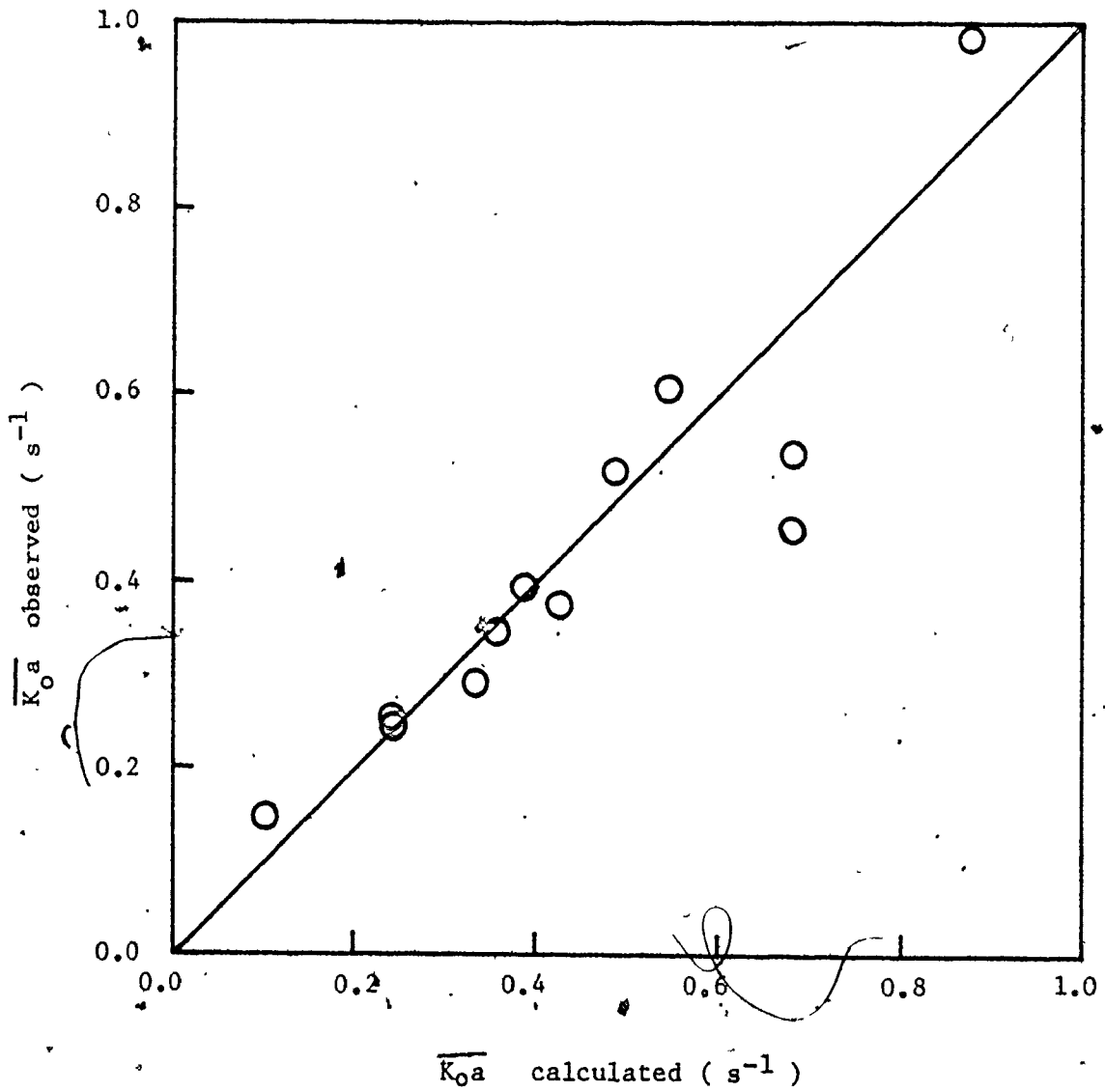


Figure 29. Comparison of $\overline{K_0a}$ observed (Karr data) with $\overline{K_0a}$ calculated.

depending on the sampling and analysis procedure. In this respect, the indicator colour change technique has an advantage in reliable measurement of column performance.

CHAPTER 7

CONCLUSIONS AND RECOMMENDATIONS

The time-averaged pressure drop in the column is substantially increased by increasing reciprocation frequency at a given flow rate. The quasi-steady model developed in Appendix A is useful in the approximate prediction of the effects of flow and frequency. The accuracy of prediction, however, is somewhat limited by the variations in effective orifice coefficient (C_o).

Reasonable agreement of observed $\overline{K_o a}$ and $\overline{K_o a}$ calculated from the model which employs the Treybal relationship is obtained at high agitation levels which are of the greatest practical interest. At low agitation, the observed $\overline{K_o a}$ tends to be much higher than the prediction from the stagnant model and agrees better with the circulating model according to which $\overline{K_o a}$ exceeds the rigid drop value by a factor of 2.56. The large deviation of experimental data from the predicted values in the absence of external agitation implies the relative importance of a collision mechanism of drop breakup and a significant entry effect.

The indicator colour change method has proven very useful in determining the averaged mass transfer rate and the local mass transfer rate in a Karr reciprocating plate

column. This method is considered to be much better than conventional sampling and analysis of exit streams. However, it is limited in application to systems for which the transferring solute can undergo instantaneous reaction with an added component.

The investigation of Karr's data has shown reasonable agreement between the observed $\overline{K}_O a$ and the $\overline{K}_O a$ predicted by a model involving the Levins rigid sphere correlation for the continuous phase mass transfer coefficient.

The models developed for cocurrent mass transfer in reciprocating plate columns, using some of the same methods that have proven useful in the development of the countercurrent mass transfer model, have been experimentally confirmed.

The usefulness of cocurrent extraction in Karr column has been shown to have several advantages such as high efficiency, high throughput, relatively uniform droplets, and flexibility of operation.

Physical properties of the system used, such as viscosity, interfacial tension and molecular diffusion coefficient, must be reliably known in order to obtain a reasonable design model. In this work, the concentration effects on properties were not considered because of the very low organic phase concentration. However, it would be useful to investigate high concentration systems in which

the interfacial tension may be considerably varied as the mass transfer takes place, for example the extraction of copper.

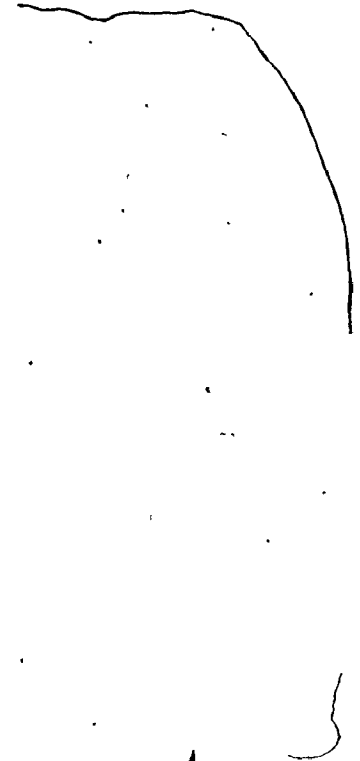
In order to investigate more reliably the local mass transfer rate, more data points should be taken in a longer column.

Finally, the indicator colour change technique is recommended for application to the countercurrent extraction processes in which the axial dispersion term in the mass balance equations must be considered. It may thus be possible to measure the mass transfer product and the axial dispersion coefficient at the same time.

REFERENCES

1. Lo, T.C., Baird, M.H.I., Kirk-Othmer; Encyclopedia of Chem. Tech., Vol. 9, 3rd Ed. (John Wiley & Sons), 1980.
2. Van Dijck, U.S. Patent 2011186, 13 Aug. 1935.
3. Karr, A.E., A.I.Ch.E. J., 5, 446 (1959).
4. Karr, A.E., Lo, T.C., Chem. Eng. Progr. 72(11), 68 (1976).
5. Sharma, R.N., Baird, M.H.I., Can. J. Chem. Eng. 56, 310 (1978).
6. Karr, A.E., Gebert, W., Wang, M., Can J. Chem. Eng. 58, 249 (1980).
7. Hafez, M.M., Baird, M.H.I., Nirdosh, I., Can. J. Chem. Eng. 57, 150 (1979).
8. Baird, M.H.I., Lane, S.J., Chem. Eng. Sci. 28, 947 (1973).
9. Kim, S.D., Baird, M.H.I., Can. J. Chem. Eng. 54, 81 (1976).
10. Hafez, M.M., Baird, M.H.I., Trans. IChem E., 56, 229 (1978).
11. Baird, M.H.I., McGinnis, R.G., Tan, G.C., Proc. Intl. Solvent Extn. Conf. (ISEC 71), The Hague, 1971, p. 251 (Society of Chemical Industry, London, 1971).
12. Hafez, M.M., Baird, M.H.I., Nirdosh, I., Proc. Intl. Solvent Extn. Conf. (ISEC 80), Belgium, 1980.
13. Astarita, G., "Mass Transfer with Chemical Reaction", Elsevier, Amsterdam, 1967.
14. Danckwerts, P.V., "Gas-Liq. Reactions", McGraw-Hill, New York 1970.
15. Northrup, E.F., Nature, 88, 463 (1912).

16. Fox, E.A., Gex, V.E., A.I.Ch.E. J., 2, 539 (1956).
17. Baird, M.H.I., Seminar delivered at Louisiana State Univ., Feb. 1981.
18. Barnea, E., Proc. Intl. Solvent Extn. Conf. (ISEC 71), 1, 347 (1971).
19. Kennedy, A.D., Pfalzgraff, C.L., Proc. Intl. Solvent Extn. Conf. (ISEC 77), 1, 333 (1977).
20. Godfrey, J.C., Slater, M.J., Chem. and Ind., 7 Oct. 745 (1978).
21. Merchuk, J.C., Shai, R., Wolf, D., Ind. Eng. Chem. Proc. Des. Dev. 19, 91 (1980).
22. Karr, A.E., Technical Report, Chem-Proc. Inc., New Jersey (1979).
23. Perry, R.H., Chilton, C.H., Chem. Engrs. Handbook, 5th Ed., McGraw-Hill.
24. Gordon, N.E., Reid, E.E., J. Phi. Chem., 26, 776 (1922).
25. Treybal, R.E., "Liq. Extraction", 2nd Ed., McGraw-Hill, New York (1963).
26. Seewald, M., M.Ch.E. Thesis, New York Univ., 1960. See also Ind. Eng. Chem. 53, 597 (1961).
27. Jealous, A.C., Johnson, R.F., Ind. & Eng. Chem. 47, 1159 (1955).
28. Mullin, J.W., Treleaven, C.R., "Symposium on Interaction between Fluid and Particles" p. 203, June 1962 (Inst. of Chem. Engrs., London).
29. Kronig, R., Brink, J.C., Appl. Sci. Res., A2, 142 (1950).
30. Handlos, A.E., Baron, T., A.I.Ch.E. J. 3, 127 (1957).
31. Laddha, G.S. and Degaleesan, T.E., "Transport Phenomena in Liquid extraction" (McGraw-Hill-Tata), 1976.
32. Korchinsky, W.J., Cruz-Pinto, J.J.C., Chem. Eng. Sci. 34, 551 (1979).

33. Ali, F.A., M.Sc. (Tech) Thesis, Univ. of Manchester (1969).
 34. Arashmid, M., Jeffreys, G.V., A.I.Ch.E. J. 26, 51 (1980).
 35. Levins, D.M., Glastonbury, J.R., Trans. Instn. Chem. Engrs. 50, 132 (1972).
 36. Jiricny, V., Prochazka, J. Chem. Eng. Sci. 35, 2237 (1980).
- 

APPENDIX A

PRESSURE DROP IN A RECIPROCATING PLATE COLUMN

Consider a Karr reciprocating plate column arrangement as shown in Fig. 3. We are interested in frictional effects on pressure loss as distinct from hydrostatic effects. Only single phase flow is considered with variation of plate oscillation as follows.

Case 1 Single phase (water) flow, plates stationary

Let the superficial velocity of the water be u_c and let the actual velocity of water through the holes be u_h . The pressure drop per plate can be calculated assuming complete loss of kinetic energy.

$$\frac{\Delta p}{n} = \frac{1}{2} \rho_c (u_h^2 - u_c^2) \quad A-1$$

The fractional open area σ for the plates is given, and the continuity equation provides

$$u_c = \sigma u_h \quad A-2$$

Hence,

$$\frac{\Delta p}{n} = \frac{1}{2} \rho_c u_c^2 \left(\frac{1 - \sigma^2}{\sigma} \right) \quad A-3$$

In practice, orifice flows usually involve a contraction which increases the pressure drop, and we rewrite equation

A-3 as

$$\Delta p = \frac{\frac{1}{2} n \rho_c u_c^2}{C_o^2} \left(\frac{1 - \sigma^2}{\sigma^2} \right) \quad \text{A-4}$$

where C_o is an orifice coefficient which is a function of Reynolds number, and approximately 0.6 at high Reynolds number.

Case 2 Single phase (water) flow; plates oscillating

Let the plate displacement be

$$Y = a \omega \sin \omega t \quad \text{A-5}$$

where

a: amplitude

ω : angular frequency ($2\pi f$)

The plate velocity is therefore

$$\dot{Y} = a \omega \cos \omega t \quad \text{A-6}$$

Now consider the continuity of water flow between the open column and a section adjacent to a plate.

$$\dot{Y}(1-\sigma) + \sigma u_h = u_c \quad \text{A-7}$$

The instantaneous pressure drop will consist of a frictional component plus an inertial component due to the acceleration of the flow.

The flow accelerates alternately in opposite directions, so we neglect the time-averaged inertial pressure, but we are interested in the time averaged frictional

pressure.

Equation A-1 cannot be applied in the same form to the oscillating plate situation because the sign of Δp will depend on the sign of the velocity u_h . Therefore we must write;

$$\frac{\Delta p_f}{n} = \frac{1}{2} \rho_c (u_h |u_h| - u_c^2) \quad \text{A-8}$$

From equations A-6 and A-7

$$u_h = u_c (1 - V \cos \omega t) / \sigma \quad \text{A-9}$$

where

$$V = a\omega (1 - \sigma) / u_c$$

Now substituting for u_h in equation A-8

$$\frac{\Delta p_f}{n} = \frac{1}{2} \rho_c u_c^2 \left\{ \frac{(1 - V \cos \omega t) |1 - V \cos \omega t|}{\sigma^2} - 1 \right\} \quad \text{A-10}$$

The time-averaged frictional pressure drop is (thus

$$\Delta \bar{p}_f = \frac{1}{2} \frac{n \rho_c u_c^2}{C_o^2} \left\{ \frac{(1 - V \cos \omega t) |1 - V \cos \omega t|}{\sigma^2} - 1 \right\} \quad \text{A-11}$$

The factor C_o has been included here but it may vary depending on the flow rate and plate oscillation frequency or amplitude.

i) Special Case of Small Oscillations (no flow reversal)

Consider the case where $V < 1$. In this case, u_h is always positive and the modulus expression in equation A-8 is not needed. Then we can simply write

$$\begin{aligned} \frac{\Delta \bar{p}_f}{n} &= \frac{1}{2} \rho_c \overline{\{u_h^2 - u_c^2\}} \\ &= \frac{1}{2} \rho_c u_c^2 \left\{ \frac{(1 - V \cos \omega t)^2}{\sigma^2} - 1 \right\} \end{aligned} \quad \text{A-12}$$

The time-averaged value of $(1 - V \cos \omega t)^2$ is

$$\int_0^\pi (1 - V \cos \omega t)^2 d(\omega t) / \pi = 1 + V^2/2 \quad \text{A-13}$$

Hence from equation A-12

$$\frac{\Delta \bar{p}_f}{n} = \frac{1}{2} \rho_c u_c^2 \left\{ \frac{1 - \sigma^2}{\sigma^2} + \frac{V^2}{2\sigma^2} \right\} \quad \text{A-14}$$

Again, inserting the orifice factor and rearranging give

$$\Delta \bar{p}_f = \frac{n \rho_c u_c^2}{2 C_o^2} \left\{ \frac{1 - \sigma^2}{\sigma^2} + \frac{V^2}{2\sigma^2} \right\} \quad \text{A-15}$$

Note that as $V \rightarrow 0$, (i.e. unpulsed case) we obtain the result of equation A-4. Equation A-15 indicates that a plot of $\Delta \bar{p}_f$ against the square of frequency should be linear, and this forms the basis of Fig. 13.

ii) Special case of Large Oscillations, $V \gg 1$

A general solution of the time-averaged value of

$$(1 - V \cos \omega t) |1 - V \cos \omega t|$$

is given by

$$\begin{aligned} \overline{(1 - V \cos \omega t) |1 - V \cos \omega t|} &= (1 + \frac{1}{2} V^2) - \frac{2}{\pi} \left\{ (1 + \frac{1}{2} V^2) \omega t_1 \right. \\ &\quad \left. - 2V \sin \omega t_1 + \frac{V^2}{4} \sin 2\omega t_1 \right\} \end{aligned} \quad \text{A-16}$$

where

$$\omega t_1 = \cos^{-1} \left(\frac{1}{V} \right)$$

Substituting equation A-16 in equation A-11 provides

$$\Delta \bar{p}_f = \frac{n \rho_c u_c^2}{2 C_o^2} \left\{ \frac{\overline{f(\omega t_1)}}{\sigma^2} - 1 \right\} \quad \text{A-17}$$

where

$$\overline{f(\omega t_1)}$$

is right hand side of equation A-16. When $V \gg 1$, equation A-17 can be simplified by

$$\Delta \bar{p}_f = \frac{n \rho_c u_c^2}{2 C_o^2} \left\{ \frac{4V}{\pi \sigma^2} - 1 \right\} \quad \text{A-18}$$

For this special case ($V \gg 1$), $\Delta \bar{p}_f$ is proportional to frequency for a given u_c and amplitude.

iii) Flow Reversal Criterion

In order that u_h can have an opposite sign to u_c , V must exceed unity (equation A-9). It follows that flow reversal can occur only when $\omega(1-\sigma) > u_c$, i.e.

$$f > \frac{u_c}{2\pi a(1-\sigma)}$$

APPENDIX B

THE EFFECT OF COALESCENCE ON DROPLET BREAKUP

A quantitative comparison of total energy dissipation per unit volume with the minimum energy required to overcome the interfacial tension is considered as follows. Let the equilibrium droplet diameter be d_p at steady condition. The minimum energy per unit volume of dispersion required to overcome the interfacial tension and prevent coalescence is estimated from the interfacial tension of the system and the specific surface area. This can be divided by the contact time ($Z/(u_o + u_A)$) to give a minimum power' per volume:

$$\psi_i = \dot{\gamma} \cdot a(u_o + u_A)/Z \quad \text{B-1}$$

Using the Eq. 5-17 for the specific surface area, then

$$\psi_i = \frac{6}{0.36} \cdot \frac{u_o \bar{\rho}^{-0.2} \gamma^{0.4}}{Z} \cdot \left\{ \frac{\bar{\rho} (1 - \sigma^2)}{h C_o^2 \sigma^2} \left[\frac{2\pi^2}{3} (Af)^3 + \frac{1}{2} (u_o + u_A)^3 \right] \right\}^{0.4} \quad \text{B-2}$$

The total hydrodynamic energy dissipation per unit volume is given by Eq. 5-15

$$\psi = \frac{\bar{\rho}}{h} \left(\frac{1 - \sigma^2}{C_o^2 \sigma^2} \right) \left[\frac{2\pi^2}{3} (Af)^3 + \frac{1}{2} (u_o + u_A)^3 \right] \quad \text{5-15}$$

As the ratio of applied energy ψ to minimum energy ψ_i is increased, the effect of droplet coalescence will progressively decrease. Some calculations of the ratio (ψ/ψ_i) indicate that the ratio is in the order of 10 at low agitation, but much larger than 100 under well agitated conditions.

U

APPENDIX C
LIST OF TABLES

Table 1 Physical Properties of MaterialsPhysical Properties at $10^{\circ}\text{C} \pm 1^{\circ}\text{C}$ ValuesDensity, ρ (kg m^{-3})

Tap water	998.00
Distilled water	998.23
Kerosene	798.00
Acetic acid	1071.4
O-xylene ^c	881.0 ¹⁵
Tridecane ^a	765.0

Viscosity^a, μ ($\text{mPa}\cdot\text{s}$)

Tap water	1.01
Kerosene	3.03
O-xylene ^c	0.88 ¹⁵
Tridencane	2.35

Interfacial tension, γ ($\text{mN}\cdot\text{m}^{-1}$)

Tap water/kerosene	34.0
water/O-xylene ^c	25.0 ¹⁵
water/tridecane ^a	27.8

Diffusion coefficient^b, D_{AB} (m^2/s)

Acetic acid/tridecane	0.99×10^{-9}
Acetic acid/O-xylene	2.06×10^{-9}

- ^a From Perry and Chilton (23) and other values are measured.
^b Calculated using Wilke-Chang correlation (23), it must be noted that the diffusion coefficient of acetic acid/tridecane was used assuming that kerosene has same physical properties as tridecane has.
^c From Karr data (22)

Table 2 List of Valves and Pumps, and Their Use

Functions	Valves	K1	K2	K3	K4	K5	K6	W1	W2	I1	C1	D1	D2	D3	D4	D5	P1	P2
Water flow only		X	X	X	X	X	X	O	O	X	X	X	X	X	X	X	X	X
Kerosene flow only		O	O	O	X	X	X	X	X	X	X	X	X	X	X	X	O	X
Preparation of organic phase by mixing		X	X	X	O	X	O	X	X	X	X	X	X	X	X	X	O	X
Return kerosene to overhead tank		O	X	X	O	O	O	X	X	X	X	X	X	X	X	X	O	X
Empty column after run		X	X	X	O	X	X	X	X	X	X	O	O	O	X	X	X	X
Sampling-Analysis of exit streams		O	O	O	X	X	X	O	O	X	X	X	X	X	O	X	O	X
Indicator colour change method		O	O	O	X	X	X	O	O	O	O	X	X	X	O	X	O	O
Wash out column & organic phase lines after run		X	X	X	O	X	O	O	O	X	X	X	O	O	O	O	X	X
Presaturation of kerosene with water		O	O	X	O	X	X	O	O	X	X	X	X	X	O	X	O	X

Table 3 Data of Analysis of Exit Streams

Run No.	u_o (cm/s)	u_A (cm/s)	f (Hz)	C_{O1} (mol/L)	C_{O2} (mg/L)	C_{A2} (mol/L)	M.B (%)	μ (%)	K_{Oa} (s^{-1})
SA 1	9.8	8.3	5.0	0.784	3.7×10^{-3}	0.873	- 0.2	99.5	0.36
SA 2	10.6	8.3	2.0	0.576	18.7×10^{-3}	0.734	+ 2.0	96.0	0.25
SA 3	10.2	8.3	1.0	0.334	68.9×10^{-3}	0.339	+ 3.0	79.0	0.11

4



Table 4.1 Classification of Experiment for the Indicator Colour Change Method

Run No.	Symbol	u_A (cm/s)	u_O (cm/s)	u_S (cm/s)	f (Hz)	h (cm)	No. of Range of data z_n (cm)
ND-1	○	4.0	4.0	0.08-0.5	3.0	5.08	7 17-154
ND-2	△	4.0	2.0	0.14-0.4	3.0	5.08	6 24-125
ND-3	□	4.0	1.0	0.06-0.23	3.0	5.08	7 26-144
ND-4		10.0	7.0	0.2-0.46	3.0	5.08	3 12-38
ND-5	①	4.0	1.5-7.6	0.175	3.0	5.08	6 25-87
ND-6	X	1.55-16.6	2.0	0.223	3.0	5.08	7 82-128
ND-7	△	4.0	3.0	0.293	1.8-5.0	5.08	7 23-136
ND-8	□	0.66	0.82	0.152	3.0-4.96	5.08	4 26-65
ND-9	①	5.38	2.4-6.02	0.161	0.0	5.08	9 28-150
ND-10	○	4.0	5.55	0.14-0.33	0.0	5.08	11 16-156
ND-12		4.0	6.0	0.19-0.53	3.0	5.08	5 7-45
ND-13		4.0	2.0-4.9	0.16	5.0	2.54	3 15-41
ND-14	△	4.0	4.2-12.2	0.122	1.0	2.54	9 27-147
ND-15	○	4.0	2.3	0.12	0.45-3.5	2.54	7 16-139
ND-16	○	4.0	3.85	0.21	0.31-3.5	2.54	9 21-144
ND-17	X	2.0	2.0	0.17-0.31	3.0	2.54	5 26-94
ND-18		4.0	4.0	0.08-0.26	3.0	2.54	9 27-146
ND-20	□	4.0	3.8-9.6	0.184	0	2.54	9 26-142

Table 4.2 Data of ND-1

	u_s^* (cm/s)	z_n (cm)	$\overline{K_o a}$ (10^2 s^{-1})
$C_{ol} = 0.151 \text{ mol/L}$	0.075	17 ± 1.0	3.27
$C_s^{**} = 1.047 \text{ mol/L}$	0.200	39 ± 0.5	4.36
$u_A = 4.0 \text{ cm/s}$	0.270	55 ± 1.0	4.58
$u_o = 4.0 \text{ cm/s}$	0.375	86 ± 1.5	4.87
$f = 3.0 \text{ Hz}$	0.428	105 ± 2.0	5.14
$h = 5.08 \text{ cm}$	0.447	111 ± 2.0	5.35
	0.532	154 ± 5.0	6.59

Table 4.3 Data of ND-2

	u_s (cm/s)	z_n (cm)	$\overline{K_o a}$ (10^2 s^{-1})
$C_{ol} = 0.236 \text{ mol/L}$	0.145	24 ± 1.0	3.23
$C_s = 1.047 \text{ mol/L}$	0.195	39 ± 1.0	2.95
$u_A = 4.0 \text{ cm/s}$	0.256	55 ± 1.0	3.05
$u_o = 2.0 \text{ cm/s}$	0.322	75 ± 1.0	3.34
$f = 3.0 \text{ Hz}$	0.398	108 ± 2.0	3.98
$h = 5.08 \text{ cm}$	0.421	125 ± 2.0	4.35

* u_s : flow rate of concentrated caustic.

** C_s : Conc. of concentrated caustic solution

Table 4.4 Data of ND-3

	u_s (cm/s)	z_n (cm)	$\overline{K_o a}$ (10^2 s^{-1})
$C_{O1} = 0.236 \text{ mol/L}$	0.056	26 ± 1.0	1.08
$C_s = 1.032 \text{ mol/L}$	0.115	38 ± 1.0	1.84
$u_A = 4.0 \text{ cm/s}$	0.125	49 ± 1.0	1.62
$u_o = 1.0 \text{ cm/s}$	0.187	75 ± 1.0	2.27
$f = 3.0 \text{ Hz}$	0.213	110 ± 2.5	2.44
$h = 5.08 \text{ cm}$	0.223	132 ± 2	2.81
	0.226	144 ± 4	3.11

Table 4.5 Data of ND-4

	u_s (cm/s)	z_n (cm)	$\overline{K_o a}$ (10^2 s^{-1})
$C_{O1} = 0.236 \text{ mol/L}$	0.203	12 ± 1.5	7.93
$C_s = 1.032 \text{ mol/L}$	0.307	22 ± 2.0	6.78
$u_A = 10.0 \text{ cm/s}$	0.457	38 ± 2.0	6.19
$u_o = 7.0 \text{ cm/s}$			
$f = 3.0 \text{ Hz}$			
$h = 5.08 \text{ cm}$			

Table 4.6 Data of ND-5

	u_o (cm/s)	z_n (cm)	$\overline{K_o a}$ (10^2 s^{-1})
$C_{Ol} = 0.144 \text{ mol/L}$	1.50	87 ± 1.0	3.12
$C_s = 1.032 \text{ mol/L}$	1.60	76 ± 1.0	3.23
$u_A = 4.0 \text{ cm/s}$	2.15	56 ± 1.0	3.36
$u_s = 0.175 \text{ cm/s}$	3.35	41 ± 1.0	3.83
$f = 3.0 \text{ Hz}$	5.40	31 ± 1.0	4.62
$h = 5.08 \text{ cm}$	7.60	25 ± 2.0	5.47

Table 4.7 Data of ND-6

	u_A (cm/s)	z_n (cm)	$\overline{K_o a}$ (10^2 s^{-1})
$C_{Ol} = 0.144 \text{ mol/L}$	1.55	82 ± 1.5	4.29
$C_s = 1.068 \text{ mol/L}$	3.30	95 ± 1.0	3.71
$u_s = 0.223 \text{ cm/s}$	5.37	116 ± 2.0	3.03
$u_o = 2.0 \text{ cm/s}$	8.20	107 ± 4.0	3.29
$f = 3.0 \text{ Hz}$	9.60	124 ± 3.0	2.84
$h = 5.08 \text{ cm}$	11.10	128 ± 4.0	2.75
	16.63	121 ± 4.0	2.91

Table 4.8 Data of ND-7

	f (Hz)	z_n (cm)	$\overline{K_o a}$ (10^2 s^{-1})
$C_{O1} = 0.203 \text{ mol/L}$	1.8	136 ± 2.0	1.59
$C_s = 1.068 \text{ mol/L}$	2.0	111 ± 2.0	1.95
$u_A = 4.0 \text{ cm/s}$	2.25	96 ± 1.5	2.25
$u_o = 3.0 \text{ cm/s}$	2.6	73 ± 2.0	2.97
$u_s = 0.293 \text{ cm/s}$	3.0	57 ± 2.0	3.80
$h = 5.08 \text{ cm}$	3.9	35 ± 1.5	6.18
	5.0	23 ± 1.0	9.41

Table 4.9 Data of ND-8

	f (Hz)	z_n (cm)	$\overline{K_o a}$ (10^2 s^{-1})
$C_{O1} = 0.203 \text{ mol/L}$	3.0	65 ± 2.0	4.67
$C_s = 1.068 \text{ cm/s}$	3.5	43 ± 1.0	7.05
$u_A = 0.66 \text{ cm/s}$	4.25	33 ± 1.0	9.19
$u_o = 0.82 \text{ cm/s}$	4.94	26 ± 1.0	11.7
$u_s = 0.152 \text{ cm/s}$			
$h = 5.08 \text{ cm}$			

Table 4.10 Data of ND-9

	u_o (cm/s)	z_n (cm)	$\overline{K_o a}$ (10^2 s^{-1})
$C_{O1} = 0.203 \text{ mol/L}$	2.40	150 \pm 2.0	0.63
$C_s = 0.990 \text{ mol/L}$	2.68	131 \pm 1.0	0.71
$u_A = 5.38 \text{ cm/s}$	2.95	110 \pm 1.0	0.83
$u_s = 0.161 \text{ cm/s}$	3.20	94 \pm 1.0	0.96
$f = 0.0 \text{ Hz}$	3.60	76 \pm 2.0	1.17
$h = 5.08 \text{ cm}$	4.25	59 \pm 2.0	1.47
	4.65	48 \pm 2.0	1.79
	5.30	37 \pm 2.0	2.29
	6.02	28 \pm 2.0	3.01

Table 4.11 Data of ND-10

	u_s (cm/s)	z_n (cm)	$\overline{K_o a}$ (10^2 s^{-1})
$C_{O_1} = 0.193 \text{ mol/L}$	0.077	16 ± 2.0	2.55
$C_s = 0.990 \text{ mol/L}$	0.137	30 ± 2.0	2.50
$u_A = 4.0 \text{ cm/s}$	0.165	45 ± 2.0	2.04
$u_o = 5.55 \text{ cm/s}$	0.185	57 ± 2.0	1.82
$f = 0.0 \text{ Hz}$	0.200	68 ± 2.0	1.67
$h = 15.08 \text{ cm}$	0.228	83 ± 1.0	1.58
	0.248	99 ± 2.0	1.46
	0.273	115 ± 2.0	1.40
	0.283	122 ± 3.0	1.37
	0.307	138 ± 3.0	1.34
	0.330	156 ± 3.0	1.29

Table 4.12 Data of ND-12

	u_s (cm/s)	z_n (cm)	$\overline{K_o a}$ (10^2 s^{-1})
$C_{O1} = 0.235 \text{ mol/L}$	0.192	7 ± 2.0	12.40
$C_s = 0.990 \text{ mol/L}$	0.208	11 ± 2.0	8.61
$u_A = 4.0 \text{ cm/s}$	0.258	16 ± 2.0	7.49
$u_o = 6.0 \text{ cm/s}$	0.360	28 ± 2.0	6.24
$f = 3.0 \text{ Hz}$	0.527	45 ± 3.0	6.16

Table 4.13 Data of ND-13

	u_o (cm/s)	z_n (cm)	$\overline{K_o a}$ (10^2 s^{-1})
$C_{O1} = 0.094 \text{ mol/L}$	2.00	41 ± 1.0	13.9
$C_s = 1.107 \text{ mol/L}$	2.82	20 ± 1.0	15.6
$u_A = 4.0 \text{ cm/s}$	4.93	15 ± 1.0	15.8
$u_s = 0.16 \text{ cm/s}$			
$h = 2.54 \text{ cm}$			

Table 4.14 Data of ND-14

	u_o (cm/s)	z_n (cm)	$\overline{K_o a}$ (10^2 s^{-1})
$C_{ol} = 0.094 \text{ mol/L}$	4.20	147 ± 2.0	1.2
$C_s = 1.107 \text{ mol/L}$	4.72	123 ± 2.0	1.4
$u_A = 4.0 \text{ cm/s}$	5.34	110 ± 2.0	1.5
$u_s = 0.122 \text{ cm/s}$	7.00	80 ± 2.0	2.0
$f = 1.0 \text{ Hz}$	7.67	72 ± 2.0	2.2
$h = 2.54 \text{ cm}$	8.26	66 ± 2.0	2.3
	9.60	49 ± 2.0	3.2
	10.82	39 ± 3.0	4.0
	12.15	27 ± 2.0	5.7

Table 4.15 Data of ND-15

	f (Hz)	z_n (cm)	$\overline{K_o a}$ (10^2 s^{-1})
$C_{ol} = 0.178 \text{ mol/L}$	0.45	139 ± 2.0	0.6
$C_s = 1.107 \text{ mol/L}$	0.68	128 ± 1.0	0.7
$u_A = 4.0 \text{ cm/s}$	1.15	95 ± 1.0	1.0
$u_o = 2.3 \text{ cm/s}$	1.68	62 ± 2.0	1.5
$u_s = 0.12 \text{ cm/s}$	2.24	38 ± 2.0	2.3
$h = 2.54 \text{ cm}$	2.85	23 ± 1.0	3.9
	3.50	16 ± 1.0	5.6

Table 4.16 Data of ND-16

	f (Hz)	z_n (cm)	$\overline{K_o a}$ (10^2 s^{-1})
$C_{O1} = 0.178 \text{ mol/L}$	0.31	144 \pm 2.0	1.1
$C_S = 1.107 \text{ mol/L}$	0.68	126 \pm 2.0	1.3
$u_A = 4.0 \text{ cm/s}$	1.15	112 \pm 2.0	1.4
$u_O = 3.85 \text{ cm/s}$	1.68	68 \pm 2.0	2.4
$u_S = 0.208 \text{ cm/s}$	1.42	83 \pm 2.0	1.9
$h = 2.54 \text{ cm}$	1.95	56 \pm 1.0	2.8
	2.24	44 \pm 1.0	3.6
	2.85	30 \pm 1.0	5.4
	3.50	21 \pm 1.0	7.6

Table 4.17 Data of ND-17

	u_S (cm/s)	z_n (cm)	$\overline{K_o a}$ (10^2 s^{-1})
$C_{O1} = 0.178 \text{ mol/L}$	0.165	26 \pm 2.0	5.54
$C_S = 1.107 \text{ mol/L}$	0.184	33 \pm 1.0	5.15
$u_A = 2.0 \text{ cm/s}$	0.208	39 \pm 1.0	5.34
$u_O = 2.0 \text{ cm/s}$	0.258	58 \pm 1.0	5.59
$f = 3.0 \text{ Hz}$	0.308	94 \pm 2.0	6.73
$h = 2.54 \text{ cm}$			

Table 4.18 Data of ND-18

	u_s (cm/s)	z_n (cm)	$\overline{K_o a}$ (10^2 s^{-1})
$C_{ol} = 0.097 \text{ mol/L}$	0.255	146 \pm 5.0	3.91
$C_s = 1.156 \text{ mol/L}$	0.227	104 \pm 3.0	4.34
$u_A = 4.0 \text{ cm/s}$	0.202	80 \pm 3.0	4.60
$u_o = 4.0 \text{ cm/s}$	0.184	56 \pm 1.0	5.68
$f = 3.0 \text{ Hz}$	0.167	47 \pm 1.0	5.86
$h = 2.54 \text{ cm}$	0.145	40 \pm 1.0	5.66
	0.133	36 \pm 1.0	5.61
	0.108	32 \pm 1.0	4.85
	0.077	27 \pm 1.0	3.86

Table 4.19 Data of ND-20

	u_o (cm/s)	z_n (cm)	$\overline{K_o a}$ (10^2 s^{-1})
$C_{O1} = 0.175 \text{ mol/L}$	3.83	142 ± 1.0	1.03
$C_s = 1.156 \text{ mol/L}$	4.05	129 ± 1.0	1.12
$u_A = 4.0 \text{ cm/s}$	4.32	107 ± 1.0	1.33
$u_s = 0.184 \text{ cm/s}$	4.85	88 ± 1.0	1.59
$f = 0.0 \text{ Hz}$	5.50	69 ± 1.0	1.99
$h = 2.54 \text{ cm}$	6.35	61 ± 1.0	2.21
	7.00	52 ± 2.0	2.57
	8.32	36 ± 2.0	3.65
	9.60	26 ± 2.0	5.00

Table 5 Cocurrent Extraction Data for the O-xylene-Acetic Acid
- Water System Obtained by Karr

Run No.	u_t^{**} (cm/s)	stroke (A) (cm)	frequency (f) (Hz)	Height of plate stack (m)	stage efficiency (%)	K_{Oa}^* (s^{-1})
K1	22.9	2.54	6.67	0.61	74.4	0.256
K2	22.9	4.45	6.67	0.61	91.2	0.456
K3	22.9	3.18	6.67	0.61	84.2	0.348
K5	22.9	2.54	3.34	0.91	69.4	0.149
K6	22.9	2.54	6.67	0.91	85.8	0.246
K7	22.9	4.45	6.67	0.91	98.6	0.537
K8	22.9	3.49	6.67	0.91	94.9	0.374
K9	42.6	3.49	6.67	0.91	92.5	0.606
K10	52.5	4.45	6.67	0.91	96.7	0.384
K11	5.79	3.18	6.67	0.91	100	0.231
K12	42.6	3.18	6.67	1.22	94.8	0.516
K13	42.6	2.54	6.67	1.22	89.4	0.392

* Calculated by Equation 6-8.

** Total flow rate.